A Search for Trojan Asteroids in Kepler Data

John J. Dolan
University of Warwick
Supervisor: Prof. Don Pollacco

July 15, 2018

Contents

Acknowledgements **1**

Abstract **1**

Preface **1**

1 Introduction **2**
- 1.1 Extra-Solar Planets . . . 2
- 1.2 Trojan Asteroids . . . 5
  - 1.2.1 Solar System Trojans . . . 6
  - 1.2.2 Exoplanetary Trojans . . . 8
- 1.3 Kepler Space Telescope . . . 11
- 1.4 Previous Studies . . . 12

2 Theoretical work **14**
- 2.1 Stability of Trojan bodies . . . 14
- 2.2 Detectability of Trojans in Exoplanetary systems . . . 19

3 Method **26**
- 3.1 Data Acquisition . . . 26
- 3.2 Removing other planets in multi-planetary transits . . . 26
- 3.3 Phase folding and visual analysis . . . 27
- 3.4 BLS analysis . . . 29
- 3.5 Fourier Analysis . . . 33

4 Results **41**
- 4.1 Phase folding and visual inspection results . . . 41
- 4.2 Fourier analysis results . . . 44

5 Conclusion **46**

List of Figures

1.2.1 Schematic of Roche potential for the Sun, Earth and Moon system. Credit: map.gsfc.nasa.gov 6
1.2.2 Schematic of Jupiters L4 and L5 Lagrange points 7
1.2.3 Trojan formation Surface density models 9
1.2.4 Hydrodynamic simulation of Trojan planet formation 9
1.3.1 Kepler CCD array with 42 single CCD sensors. Credit: nasa.gov 11
1.4.1 Hippke, Angerhausen trojan plot 13

2.1.1 Trojan stability models 16
2.1.2 Trojan libration amplitude models 18
2.2.1 Phase folded injected trojan planet (non-librating model) 22
2.2.2 Phase folded injected Trojan planet (librating model) 23
2.2.3 Phase folded injected Trojan swarm at L4 and L5 24
2.2.4 Schematic showing the angular extent of large Trojan swarm. Not to scale. Trojan swarm may appear out of transit with respect to the planet. This would produce only a fraction of the dimming expected if the entire swarm were transiting. 25

3.3.1 Running Median filter 28
3.4.1 BLS periodogram of Trojan planet 30
3.4.2 BLS periodogram of Trojan swarm 31
3.5.1 Data window of Kepler 628b 34
3.5.2 Fourier coefficient amplitude 36
3.5.3 Cleaned a_n cosine coefficients 37
3.5.4 Reconstructed data from cosine coefficients 38
3.5.5 Reconstructed data from sine coefficients 39

4.1.1 Example of a trojan candidate 42
4.1.2 Ramp effect 43

4.2.1 Reconstructed Fourier coefficients from Kepler 91b data 45

Acknowledgements

Foremost, I would like to express my sincere gratitude to my supervisor, Professor Don Pollacco, for giving me the opportunity to pursue my dream career as an exoplanetary researcher and his encouraging words of wisdom throughout the past year. I enjoyed every minute of it.

I would also like to thank the experts who were extremely helpful in this research project: Dr. Dimitri Veras, Dr. Paul Chote, Dr. David Armstrong and Prof. Tom Marsh. Without their passionate participation and input, this research could not have been successfully conducted.

I would also like to acknowledge Dr. Peter Wheatley as the second reader of this thesis, and I am gratefully indebted for his very valuable comments on this thesis.

I would particularly like to thank my office buddy, Conor Talbot, for his assistance, supportive comments and suggestions, and intellectual discussions throughout the past year.

To my wife, Sarah, and her family. Thank you for the guidance and support you have given me this past year. For this, I am very grateful.

Finally, I must express my profound gratitude to my eternal cheerleaders, my parents. Thank you for providing me with unending support and continuous encouragement throughout my years of study and through the process of researching and writing this thesis. This accomplishment would not have been possible without you.

Thank you.

Abstract

Context: Trojan asteroids are asteroids that become trapped at the L4 and L5 Lagrange points of their respective planet-star system. These Lagrange points, first proposed by Italian Mathematician and Astronomer, Joseph Lagrange, are gravitationally stable regions in the planet-star system where the gravitational effects of the planet and the star cancel out, allowing debris to congregate at these Lagrange points. Trojan asteroids accompany almost every planet in our own solar system and perhaps, exoplanetary systems. Kepler has detected several thousand extrasolar planets to date, yet only a handful of studies have been dedicated to search for these exo-Trojan asteroids/planets. Finding such small bodies in extrasolar systems may further our understanding of planetary formation.
Aim: The aim of this project is to detect large transiting trojan asteroid clouds or, potentially, trojan planets in the Kepler dataset.
Method: Using a variety of statistical signal processing techniques, such as phase folding analysis, BLS periodogram and Fourier analysis, I search for statistically significant dips in stellar flux caused by a transiting trojan swarm or individual large trojan body.
Conclusion: Upon analysing the Kepler dataset in detail with a variety of methods, no significant trojan transit feature was detected. However, some insight has been provided as to how longer term studies may be able to detect trojan bodies at larger orbital radii with more massive planetary hosts. The Fourier method described could be used with future datasets to detect exoplanetary rings and, potentially, large trojan swarms.

Preface

Since the first discovery of an exoplanet around a main sequence star (Mayor and Queloz, 1995), astronomers have found over 3500 planets outside our solar system as of August 2017 (see exoplanetarchive) and since then our understanding of exoplanets has advanced at a extraordinary pace. These worlds have shown us that the Earth is but one of countless billions of planets in the Universe and sheds light on the zoo of planets out there, some, similar to the Solar system planets and some, very alien.

Most of these exoplanets have been discovered via the transit method, of which, the Kepler space telescope has been dominant. Kepler targeted a region of the sky in the direction of Cygnus, one of the densest regions of sun-like stars in the Milky way (Koch et al., 2010), and took photometric measurements of approximately 150,000 stars in order to detect transiting planets.

Transiting planets are observed when a planet passes in front of its host star (with respect to the observer) and decreases the observed flux of the star. This decrease can be extremely small, on the order of 1% for a Jupiter size planet (Hellier et al., 2014) and 0.00001% for a moon size planet (Barclay et al., 2013). However, with the sensitive CCDs on board Kepler, no atmosphere to disrupt the incoming light and almost continuous stellar monitoring, Kepler has detected planets with radii smaller than the Earth. Kepler may even be sensitive enough to detect groups of Asteroid.

Chapter 1

Introduction

1.1 Extra-Solar Planets

Extra-Solar planets (or Exoplanets) are defined as planets orbiting stars other than the Sun. Of the ~3500 or so planets astronomers have discovered, many of these worlds are vastly different than planets in our own Solar System. The discovery of these planets has prompted astronomers to re-think how planetary formation operates and enriched our knowledge of the Universe (Ford, 2014).

In the 16th century, the Italian philosopher, Giordano Bruno, was one of the first to acknowledge the possibility of other worlds beyond our Solar System. Bruno was a believer in the Copernican Heliocentric theory and elaborated on it to include other heliocentric systems in the Universe. In his writings he claims “There are innumerable suns and an infinite number of planets which circle around their suns as our seven planets circle around our Sun.” We do not see planets revolving about other stars “because of their great distance or small mass” (MacLachlan). Today, with help from missions like the Kepler Space Telescope, we know that almost every star has at least one planet (Cassan et al., 2012) and one in every 6 stars has an Earth like planet orbiting it (Aguilar, 2013).

These statistics have opened up the field of Exoplanetary Science which has led to the discovery of some very strange and some very familiar worlds.

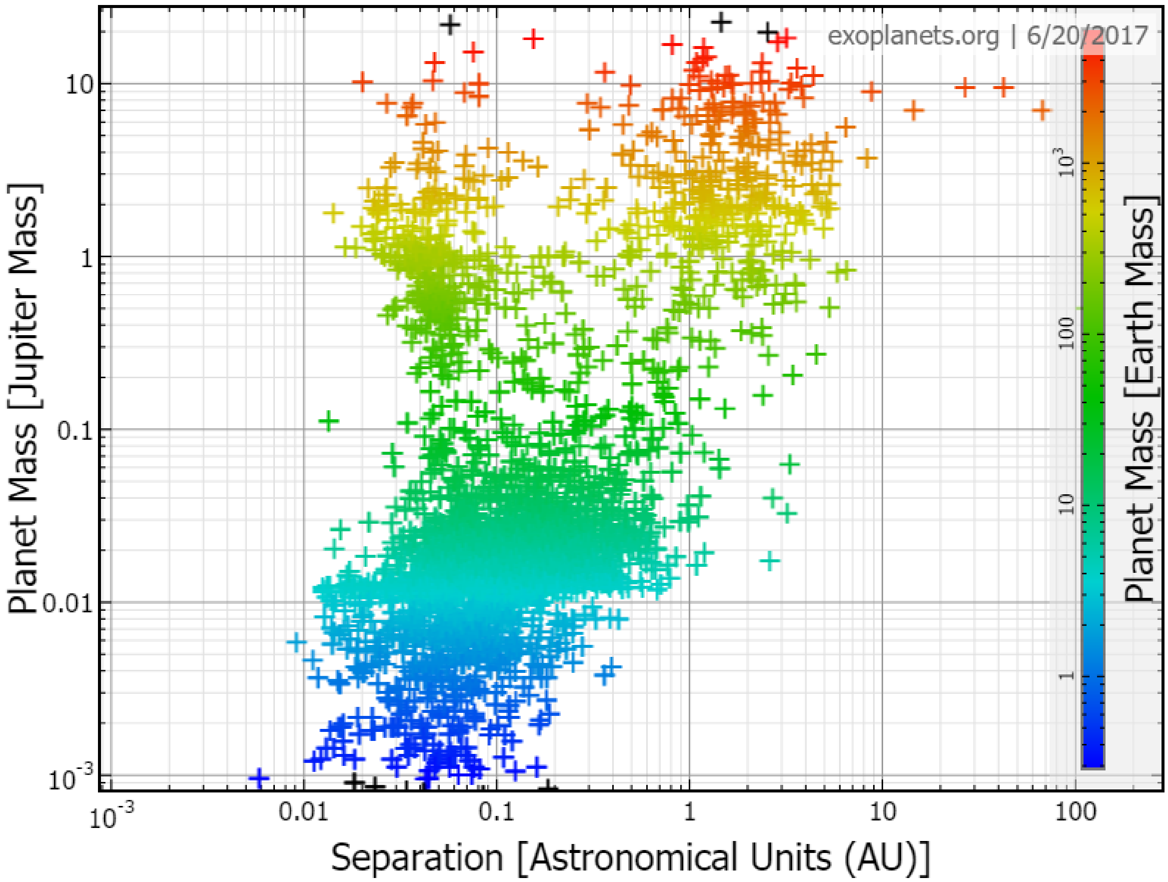

Figure 1.1.1: Distance of discovered planets from the parent star vs planet mass.

One such class of strange planets astronomers have found are the "Hot Jupiters", first discovered by Mayor and Queloz (1995). These giant planets are >10 times the radius of the Earth (Jupiter size or greater) and orbit their host star with a period ranging from a few days to a few hours (Gillon et al., 2014). Hot Jupiters can have surface temperatures of several thousand degrees Kelvin (e.g. Kelt-9b (Gaudi et al., 2017)), some having extremely bloated atmospheres leading to atmospheric stripping by the host star (Vidal-Madjar et al., 2003). The formation mechanism of these objects was unclear at first as gas giant planets can not form in such extreme temperature environments. It is now understood that Hot Jupiters form at larger orbital radii and migrate inwards toward their parent star due to interactions with the protoplanetary disk (Masset and Papaloizou, 2003). It is also possible that planet-planet scattering events can send the planet on an inward trajectory towards the host star, causing the orbital plane of the planet to be tilted with respect to the direction of stellar rotation

(Nagasawa et al., 2008). These processes are assumed to be destructive for other planets in the system, however, WASP-47b appears to be an exception. The WASP-47 system hosts a Hot Jupiter (WASP-47b) and three additional planets, 2 of which are larger orbital radii than WASP-47b. This system architecture may hint that Hot Jupiter migration may not be as destructive as once thought.

Super-Earths are a class of planets which do not exist in our solar system and thus are a planetary curiosity. These planets are the most common planet found (Kreidberg et al., 2014). With masses of 1.9 - 10$M_\oplus$ (Charbonneau et al., 2009), they are thought to have a compositional mix of rock and gas. A sub-class of this category are planets defined as mini-Neptunes. These are planets that have a potentially massive rocky core with a thick gaseous atmosphere. Kepler-10c is an example of a Super-Earth. With a radius of $2.35^{+0.090}_{-0.040}R_\oplus$ and a mass of $17^{+1.3}_{-1.20}M_\oplus$, it is one of the most massive planets expected to have a predominantly rocky composition (Dumusque et al., 2014). This type of planet is dubbed a mega-Earth.

In the search for habitable planets where life could flourish, astronomers and astrobiologists are keenly interested in terrestrial planets, or Earth-like planets. With sizes ranging from 0.8-1.25$R_\oplus$, the majority of these planets are expected to be composed mainly of rock. There are some exceptions to this, including Kepler-138d. With a radius $1.2^{+0.11}_{-0.10}$ times greater than the Earth but an estimated mass of $0.64^{+0.67}_{-0.38}M_\oplus$, this puffy planet has a large volume but relatively small mass, indicating a large atmosphere but a small rocky core (Kipping et al., 2014).

Terrestrial planets in the habitable zone are of particular interest, as they orbit their parent star at a distance where liquid water could exist on the surface (a key ingredient for life). Planets even smaller than the Earth have been detected with the Kepler Space Telescope. Kepler-37b has a diameter of $\sim$3900km, not much larger than the moon (Barclay et al., 2013). It is possible that objects even smaller than this may be hidden in the Kepler dataset, e.g. Trojan asteroid swarms or even Trojan planets.

1.2 Trojan Asteroids

When we think of asteroids, we often refer to the small, kilometer sized bodies located in the Asteroid belt between Mars and Jupiter. However, we often forget about another class of Asteroids, Trojan Asteroids. These are bodies that are trapped in the gravitationally stable region of a planets' Lagrange points, L4 and L5. Lagrange points were first proposed by the Italian/French Mathematician Joseph-Louis Lagrange, while attempting to solve the three-body problem. L4 and L5 points are located in an orbit 60° leading and 60° trailing the planet.

$$\phi = -\frac{2}{(1+q)r_1} - \frac{2q}{(1+q)r_2} - (x - \frac{q}{1+q})^2 + y^2,$$

where q is the ratio of m2/m1,

m2 and m1 are the planet and trojan masses, respectively,

and x and y are the distances from the center of mass in the x and y direction.

The Roche potential gives trojan bodies their stability in the Lagrange points. We can see in Figure 1.2.1 that the Lagrange points indicate islands of stability in the gravitational potential of a system. The Roche potential describes the balance of gravitational forces of two bodies on one (e.g. the Sun and Earth's gravitational pull on a Trojan at L4). 1.2 shows that the mass ratios of the planet and trojan are of fundamental importance to the stability of the system, we will discuss this further in Section 2.1.

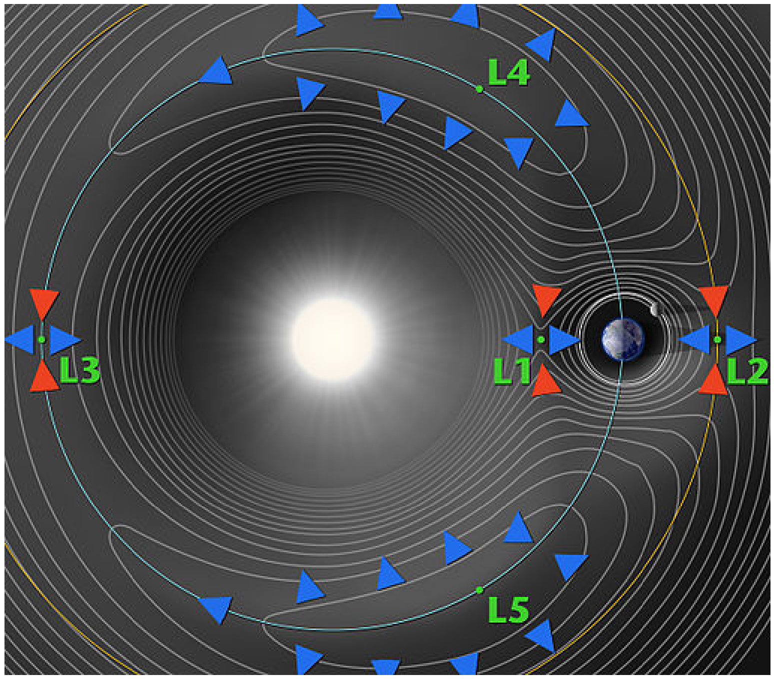

Figure 1.2.1: Schematic of Roche potential for the Sun, Earth and Moon system. Credit: map.gsfc.nasa.gov

1.2.1 Solar System Trojans

The first Trojan asteroid (588 Achilles) was discovered in 1906 by the German Astronomer, Max Wolf. Since then, astronomers have discovered many Trojans in our Solar System. Jupiter has the largest number of Trojan asteroids with 6456 discovered as of January 2017 (http://www.minorplanetcenter.net/iau /lists/JupiterTrojans.html). Neptune and Mars have a much smaller population of Trojan asteroids with 17 and 4 Trojans respectively while both the Earth and Uranus have just one detected Trojan Asteroid.

Earth's single Trojan asteroid, 2010 TK_7, has been extensively studied (Connors et al., 2011). It has an estimated diameter of ~300 meters and exhibits a chaotic orbital configuration. With an orbital inclination of 20° and an eccentricity of 0.191 (Schwarz and Dvorak, 2012), this asteroid dramatically oscillates horizontally and vertically around the Earth's Lagrange point. This libration can be so extended, that it can sometimes be found close to the opposite side of the Sun to the Earth.

Although it possesses no Trojan asteroids itself, Saturn does however have Trojan moons. Both Dione and Tethys have two Trojan companions. Helene and Polydeuces are Trojan bodies of Dione, located at its L4 and L5 points respectively, while Telesto and Calypso are located in Tethys's L4 and L5 respectively. Saturn's moon's Janus and Epimetheus are also in a co-orbital "Horseshoe" configuration. The pair "swap" orbits in an orbital dance around the Saturnian rings.

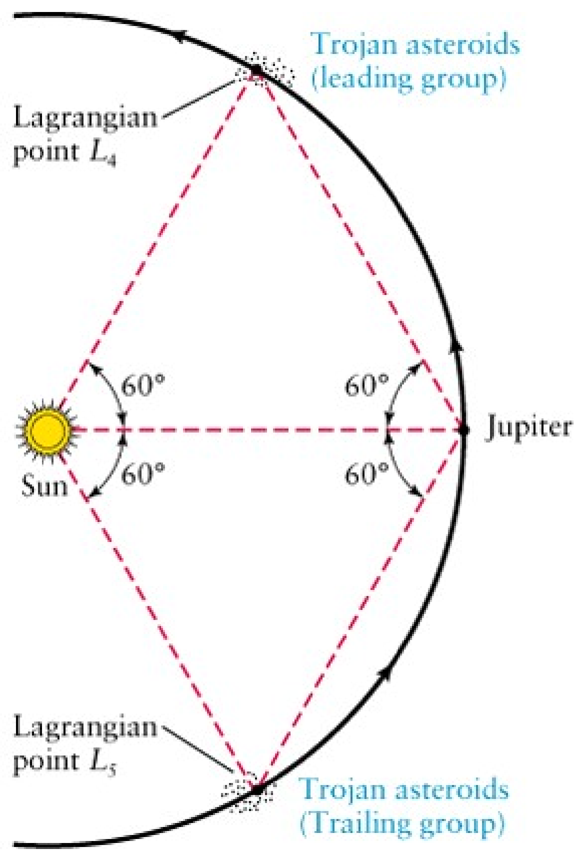

Figure 1.2.2: Schematic of Jupiters L4 and L5 Lagrange points

Neptune's known Trojans are less numerous than Jupiter's population, however it holds some of the largest Trojans in the Solar system. Almost all of the Neptunian Trojans have radii >50km and are possible captured Kuiper belt objects. Work from Sheppard and Trujillo (2010) have pointed to a potentially massive Neptunian Trojan cloud with a population comparable to Jupiter's.

It is estimated that Jupiter has many more Trojans than detected, with calculations of ~2×10^5 objects with diameters >2km and ~6×10^5 with diameters >1km (Yoshida and Nakamura, 2005). These asteroids form swarms around the L4 and L5 points, which librate around these regions with a libration amplitude of ~30° (Marzari et al. (2002), Jewitt et al. (2000)).

1.2.2 Exoplanetary Trojans

It is possible that Trojan bodies may be significantly larger in other solar systems than the Trojan asteroids we see in our Solar System (Dvorak et al., 2004; Laughlin and Chambers, 2002; Lyra et al., 2009). The largest known Trojan body is 624 Hektor which is ~239km in diameter (Fernández et al. (2003), Table 4). Laughlin and Chambers (2002) have shown that the mass ratio of a planet and a Trojan body of unity can exist in a stable, co-orbital configuration. Also, if the system is stable for long periods of time, co-orbital growth may occur, resulting in a single large body at L4 or L5, a "Trojan planets" (Cresswell and Nelson, 2009).

Migration of planets with Trojan companions may be detrimental to the stability of the Trojans themselves. Under the assumption that Hot Jupiters are formed at distances further than the snow line and migrate inwards toward the central star where they are seen today, could a Trojan Swarm or planet survive such a migration? As the planet migrates inward, so to do the associated L4 and L5 points. This could cause a breakup of the Trojan asteroid swarm or, in the case of a Trojan planet, cause a planet-planet scattering event. However, simulations from Lykawka and Horner (2010) show that, depending on how violent and when the migration occurs, giant planets may capture material in primordial disks at their respective Lagrange points as they sweep through the disk. This may imply that, under the right conditions, planetary migration may not be destructive as we think. Observations of the WASP-47 system have shown that other planets can exist in the same system as a hot Jupiter planet, meaning the stability of Trojan bodies may too be unaffected by planetary migration.

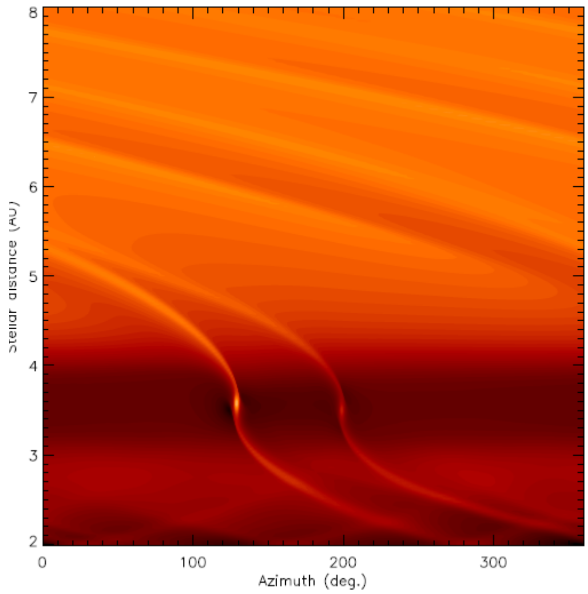

Figure 1.2.3: 2D hydrodynamic model showing the formation of a host planet with a trailing trojan planet in a protoplanetary disk. The planets masses are 156$M_\oplus$($left$) and 65$M_\oplus$ (right). Cresswell and Nelson (2009)

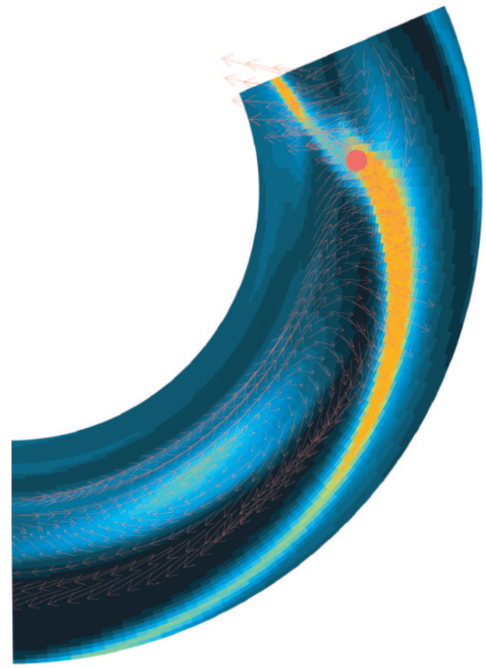

Figure 1.2.4: Hydrodynamic calculation model showing a planet clearing a gap in a disk. Vortical flow is observed in the model around the L5 point. Particle may become trapped at the L5 point and form of a second planet in a 1:1 resonance with the first planet.Laughlin and Chambers (2002)

A discovery of a Trojan swarm or planet in an exoplanetary system would assist astronomers and theorists understand the formation mechanisms of such objects and further our knowledge of the system's architecture itself. For example, it is thought that the Neptunian Trojan swarms may be a collection of captured Kuiper belt objects in a process known as "freeze in" capture. This process occurs when Neptune and Uranus migrate across a mutual 2:1 resonance and perturb the orbits of minor bodies. Once the planets become stable again, any bodies located in the Lagrange point become trapped there (Morbidelli, 2005). If a massive Trojan swarm were detected in an comparable system, this could indicate the presence of an undetected cloud of small bodies similar to the Kuiper belt that may be feeding these Trojan regions.

Similarly, A detection of Trojan asteroids in an exoplanetary system with a Hot

Jupiter would provide important constraints on the dynamical evolution of these giant exoplanets (Moldovan et al., 2010).

Combining our knowledge of Trojan asteroids in our solar system, theoretical models and data from advanced space telescopes like the Kepler space telescope, we can begin to search for these objects in other planetary systems.

1.3 Kepler Space Telescope

The Kepler space telescope was launched in 2009 with the sole purpose to search for transiting planets in other solar systems and to build a statistical profile of the population of Earth-like planets in our galaxy. On board the spacecraft is one of the most advanced CCD arrays ever launched. This CCD 'Photometer' array contains 42 single CCD chips and has a FOV of 105 square degrees, enabling it to perform wide field photometry of the Cygnus region. With a 30 minute cadence, the CCD captures light from approximately 150,000 stars with the sensitivity to detect Earth-sized planets around sun-like main sequence stars. Kepler also provided astronomers with short cadence data of 1 minute sampling to estimate transit timing variations and astroseismology.

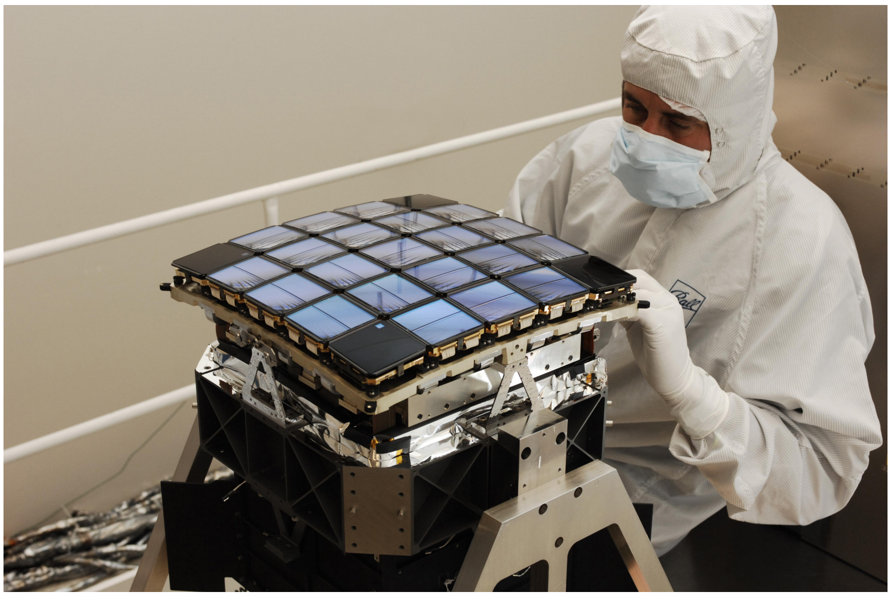

Figure 1.3.1: Kepler CCD array with 42 single CCD sensors. Credit: nasa.gov

Kepler was placed in an Earth trailing heliocentric orbit with an orbital period of around 375 days. The Kepler mission ended in May 2013 after the failure of its second reaction wheel. However, Kepler remains operational today under the K2 mission, and continues to detect transiting exoplanets (Fridlund et al., 2017). As of July 2017, the K2 mission has detected 323 confirmed planets along with 479 planet candidates (see exoplanetarchive).

1.4 Previous Studies

Attempts have been made to find such Trojan objects in exoplanetary systems. Moldovan et al. (2010) used photometric data from the MOST mission to search for Trojan-like transit signals at the Lagrange points of the hot Jupiter, HD209458b. With a 10 second cadence, over 13 days of continuous observation and a sensitivity of ~1 Lunar radius, the MOST telescope provided excellent data to search for Trojan-like transits in this system. However, no convincing evidence was found to support any transiting Trojans.

Janson (2013) also find no significant Trojan candidates with Kepler data. By creating a "river diagram" for each KOI, the author searched for librating objects around the L4 and L5 points using a search algorithm and visual inspection.

Previous claims have been made on the detection of a Trojan planet in the Kepler-223 system. In 2011, KOI 730.03 (later named Kepler 223e) was claimed to be a Trojan planet of KOI 730.02, sharing the same orbit at the L5 Lagrange point (Lissauer et al., 2011). The paper was later retracted after further analysis revealed the planets were in a 2:1 resonance, not 1:1.

Placek et al. (2015) also report a possible exo-Trojan planet in the Kepler 91 system. Lightcurves reveal Trojan-like dips at L5 in the orbit of Kepler 91b, a short period hot Jupiter. Further testing is required to validate this claim, but if this is confirmed it will force astronomers to re-think how destructive hot Jupiter migration may be.

The most tentative results have come from work done by Hippke and Angerhausen (2015). They show a 2σ confidence level of a detection of an overall Trojan population with their "Superstack" method. This method required phase folding lightcurves of confirmed planets and planet candidates to search for transit signals at L4 and L5 from an median averaged sample of light curves. They chose only phased lightcurves with dips in flux at L4 (Phase ~ 0.33) and L5 (Phase ~ 0.66) where the primary transit is set to occur at phase 0.5.

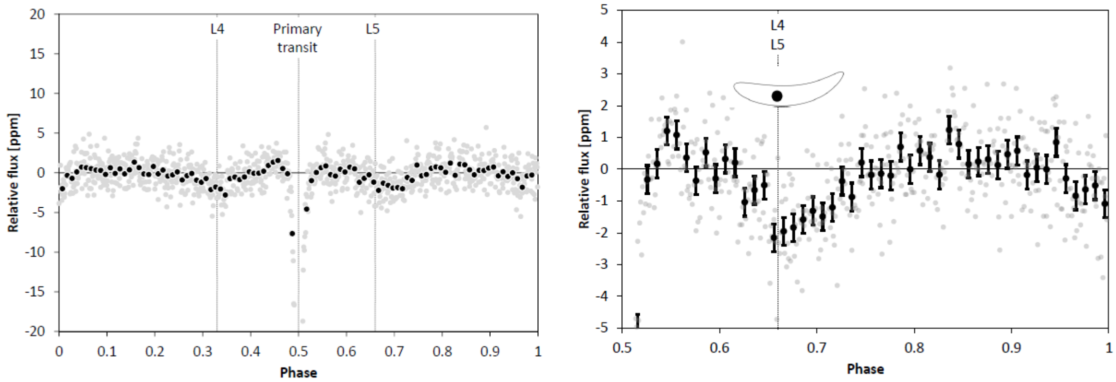

Figure 1.4.1: Sub-sample superstack in normal (left) and symmetrically folded (right) phase fold, with expected orbit size shown for reference. Note different vertical axes. Gray dots are 1,000 bins over phase space, black dots with error bars (right) are 100 bins for better visibility. (Hippke and Angerhausen, 2015)

The median averaged lightcurves of 1940 confirmed Kepler objects and KOI's exhibits a structured dip in flux at L4 and L5. An estimate of an average Trojan dip of 2ppm (parts per million) was made, which would be equivalent to a 970km radius single object. A density estimate is made for Trojan-like dips with varying period. The indications here are that Trojans may be uncommon with semi-major periods <60days. The authors attribute this to possible radiation effects (Yarkovsky effect), which may cause orbital perturbations of Trojans closer to their parent star. However, although the Yarkovsky effect is known to influence main belt asteroids, it is unclear how stellar radiation affects the stability of Trojan asteroids.

Chapter 2

Theoretical work

2.1 Stability of Trojan bodies

When searching for Trojan objects in exoplanetary systems, it is important to understand the stability criteria for these bodies to assess whether these bodies can exist in the L4/L5 positions of a Hot Jupiter, for example.

To test what the limits of stability in planetary systems with Trojan planets or large swarms, I perform an analysis using the following stability criteria (Deprit and Deprit-Bartholome, 1967):

$$27((m_1 * m_2) + (m_2 * m_3) + (m_3 * m_1)) < (m_1 + m_2 + m_3)^2$$
$$=> Stable$$

where m_1 is the stellar mass, m_2 is the planetary mass and m_3 is the mass of the Trojan.

Using this criteria, we can test what ratios of planet, star and Trojan masses should be stable. The results from this analysis can be seen in Figure 2.1.1. The plots show varying masses of Trojan and host planet (in Jupiter masses) with the top plot representing a $0.5M_\odot$ star in the system, middle plot representing a $1M_\odot$ star in the system and the bottom figure having a $2M_\odot$ star in the system. The unstable regions are marked as red dots while stable regions are marked in blue dots. The green lines show where the mass limit is for a Deuterium burning Brown Dwarf (i.e. anything higher than the green line ($>13M_J$) represents a brown dwarf). The host planet and trojan planet masses are set to be 0.5-$15M_J$ in steps of $0.5M_J$.

Unsurprisingly, we see that the lower mass stars have stricter mass criteria for stability, allowing ‘only’ a 4 Jupiter mass Trojan and 4 Jupiter mass planet to be in a stable configuration. This result also tells us that we should not expect to see any Trojans in a system with an orbiting massive (>20-30 Jupiter masses) brown dwarf or binary star system for example. However, this also shows, for any given planet less massive than a brown dwarf in an exoplanetary system, the L4/L5 configuration is stable.

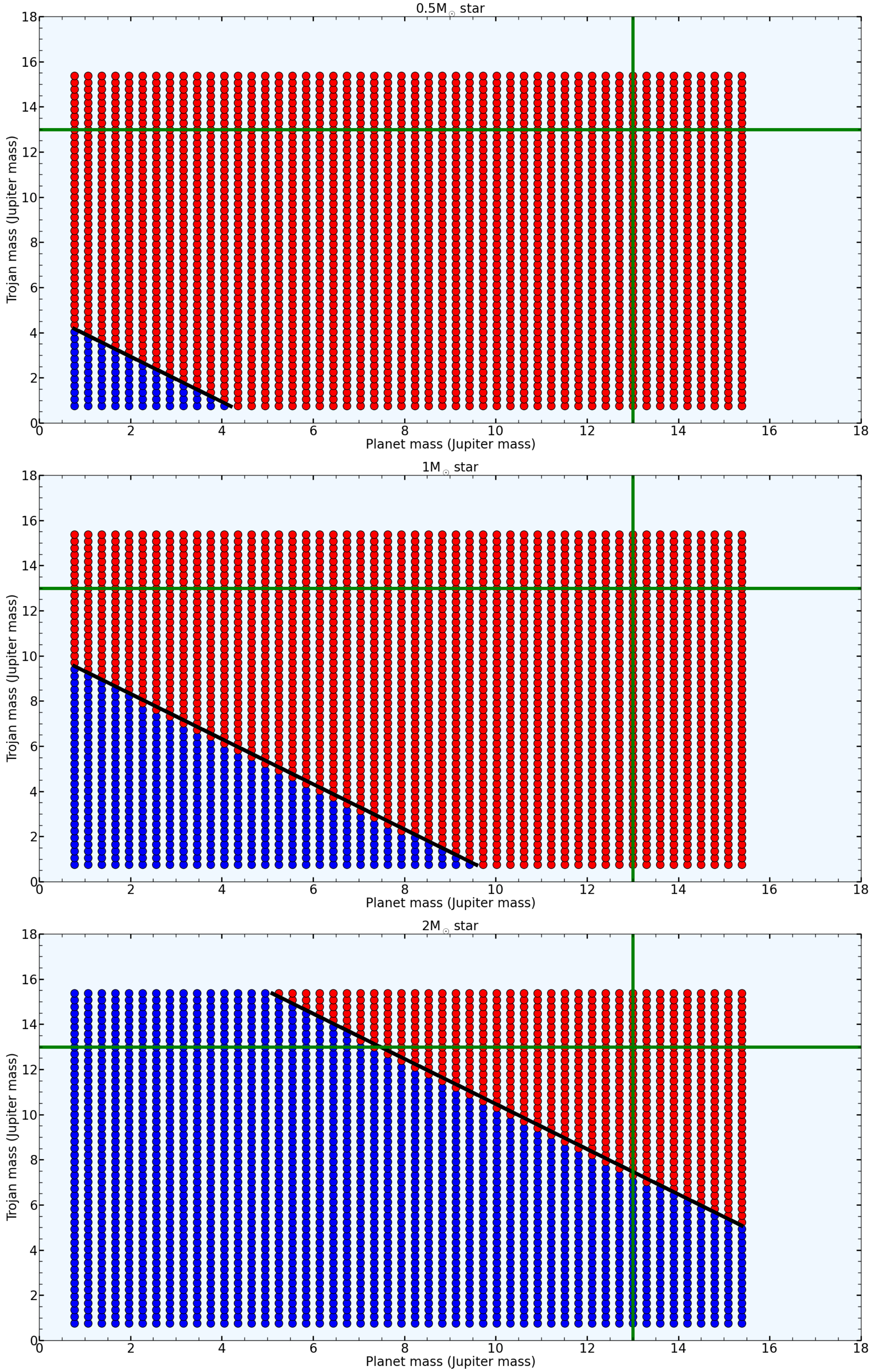

Figure 2.1.1: Stability models using planet and Trojan masses of 0.5-15M_{Jup} with stellar masses of 0.5,1 and 2$M_{\odot}$. Red dots indicate unstable planet-Trojan mass ratios and blue dots represent stable planet-Trojan mass ratios

One problem in detecting Trojans may arise when we consider libration, in particular Trojan planets. Trojans are not stationary bodies, but librate around their respective L4 and L5 points. This includes a stable region in which the planet may transit but a Trojan planet may librate above or below the orbital plane of the host planet, thus may not transit the star. It may be possible that some of the ~3000 planets (and planet candidates) we have discovered so far may actually be Trojan planets. The primary planet may be inclined to our line of sight and thus only the trojan planet transits the star (Janson, 2013). Trojan libration periods can range from days to hundreds of years. The libration period is proportional to the mass ratio of the Trojan, planet and host star and the orbital period of the primary planet (Marzari et al., 2002).

$$T_t = T_p\sqrt{\frac{4\ m_1}{27(m_2 + m_3)}} \tag{2.1.1}$$

where T_t is the libration period of the Trojan, T_p is the orbital period of the planet, m_1 is the mass of star, m_2 is the mass of planet and m_3 is the mass of Trojan.

We can see from equation (2.1.1) the libration period (and therefore the libration amplitude) is dependent on the masses of all 3 bodies and the orbital period of the parent planet. Using equation 2.1.1, we can test the upper limit of the libration amplitudes (or libration periods) of Trojans to a first order approximation. In Figure 2.1.2, we see this upper limit of libration amplitudes for varying planet mass with Trojan masses with orbital periods of the host planets, given a $1M_\odot$ star. Here, we see that, given the same mass host planet, varying Trojan masses give very different libration periods with the smaller Trojans taking longer to complete their epicyclic motion around L4/L5. We can also see that the mass of the host planet is an indicator of Trojan libration period. The more massive the host planet, the shorter the libration period. This is probably due to the deeper potential wells of the Lagrange points created by the massive host planet. Lower mass planets will create “shallower” Lagrange point gravitational potential wells and therefore should host less Trojan material.

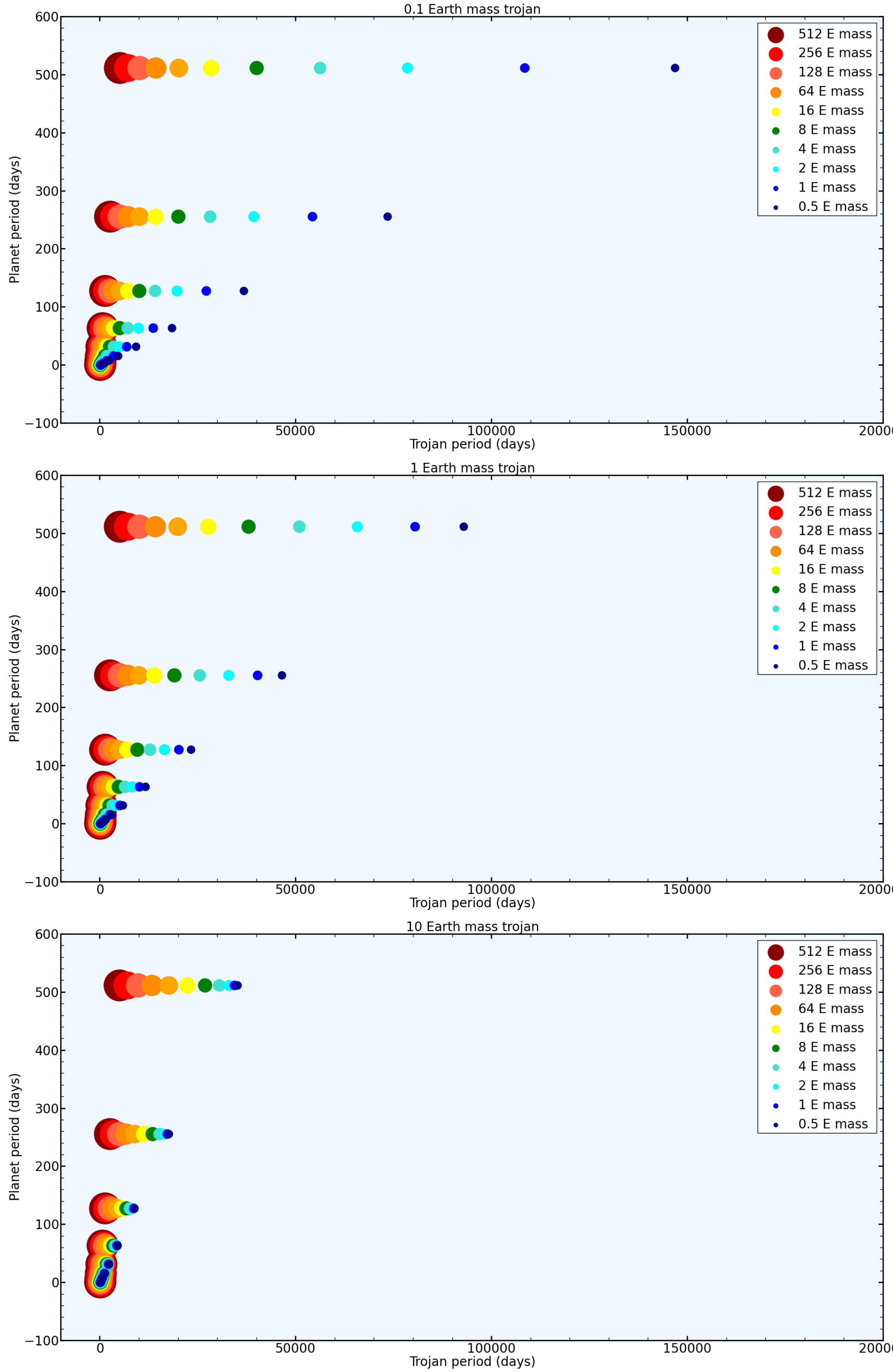

Figure 2.1.2: Models of Trojan libration periods/amplitudes. These models show that larger mass Trojan bodies should have smaller libration amplitudes and thus be more 'settled' in the the Lagrange point. These models were created with Trojans of 0.5,1 and 10$M_{\oplus}$.

2.2 Detectability of Trojans in Exoplanetary systems

Trojan Asteroids can be small, less than a km across. Individual Trojan asteroids, like those in our Solar system, would not be detectable in other planetary systems with our current instruments. However, Jupiter's Trojan population are so numerous that collectively the L4 swarm alone could form an equivalent solid sphere around 400-600km across (assuming a bulk density of 2000kg $m^{-}3$) (Jewitt et al. (2000), Hippke and Angerhausen (2015)).The combined known Neptunian Trojan population would have a transiting area equivalent to 545km in radius (assuming a bulk density of 2000kg $m^{-}3$). Trojans may be much larger in other solar systems. Individual small bodies could combine to form planet sized objects, or a planet could be captured in the L4/L5 point of a larger host planet.

$$\begin{aligned} \Delta F &= \left(\frac{R_{\text{planet}}}{R_{\text{star}}}\right)^2 \\ \Delta F &= \left(\frac{600\text{km}}{695500\text{km}}\right)^2 \\ \Delta F &= 0.75\text{ppm} \end{aligned} \tag{2.1}$$

A single 600km diameter (or an equivalent area) trojan
would be below Keplers detectable range for a 1 solar radius star.

Although the Jovian Trojan population would not be detectable in the Kepler dataset, models have also shown that even larger bodies may exist in these 1:1 co orbital resonances, even as large as Saturn (Cresswell and Nelson, 2009). It may also be possible to detect large Trojan swarms themselves. The probability of detecting Trojans may be easier in very young systems where the primordial material has not yet dissipated (Moldovan et al., 2010).

Kepler has the ability to detect dips in stellar flux to a level of 20ppm at 12th magnitude over 6.5 hours (Batalha, 2014). This high precision photometry has aided in the discovery of some of the smallest planets we know today (Barclay et al., 2013). One such planet, Kepler 37b, is estimated to be approximately the size of Earth's moon. If such a body were located in the gravitational potential of L4 or L5, it should be detectable (assuming small libration amplitudes). It is reasonable to assume that exoplanets may host Trojan objects larger than Kepler 37b and may be hidden in the Kepler dataset (Cresswell and Nelson, 2009; Laughlin and Chambers, 2002).

Given Kepler's 20ppm sensitivity, we can estimate the size of a trojan swarm Kepler could detect (see equation 2.2).

$$\begin{gathered}
\left(\frac{R_{\text{planet}}}{R_{\text{star}}}\right)^2 = \Delta F \\
\frac{A_{\text{Trojan}}}{A_{\text{star}}} > 20 \text{ x } 10^{-6} \\
A_{\text{star}} = 1R_{\odot} = 1.5205261 \text{ x } 10^{12}\text{km}^2 \\
=> A_{\text{Trojan}} = 30410522\text{km}^2 \\
=> R_{\text{Trojan}} = \sim 3000\text{km} \\
\text{(assuming single large Trojan)}
\end{gathered} \tag{2.2}$$

An object or swarm of objects with a area area of ~$3\text{x}10^7\text{km}^2$ would be visible in the Kepler time series data of quiet main sequence stars of $1\text{R}_{\odot}$. Trojan asteroid swarms at L4 and L5 would be seen at an orbital phase ±60° either side of the planet transit signal in the Kepler dataset (Janson, 2013).

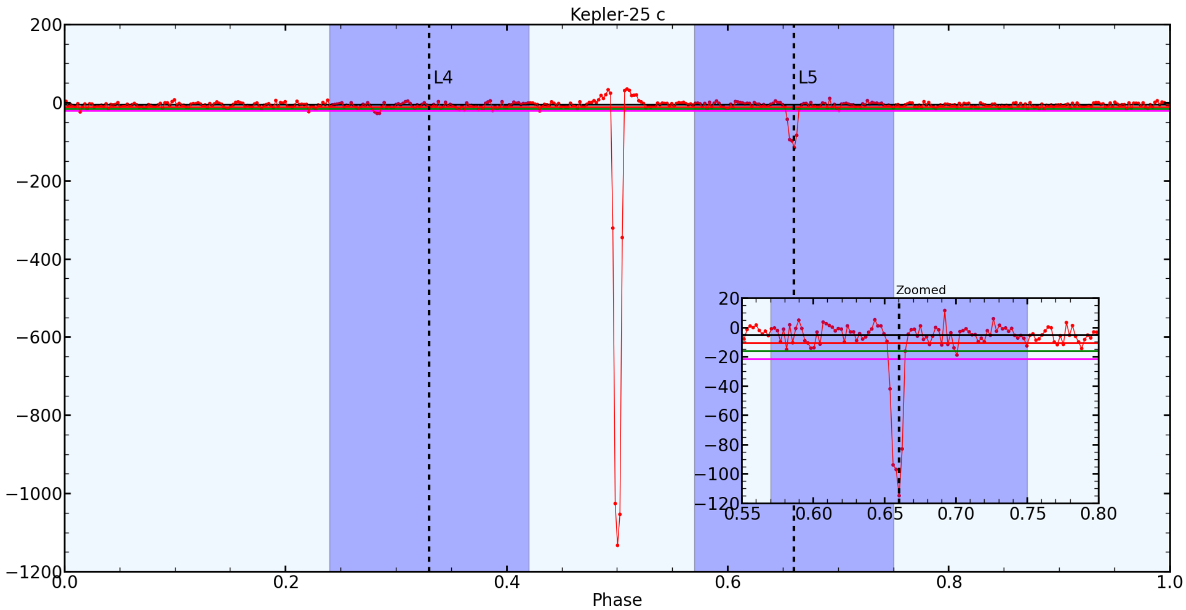

Figure 2.2.1: Injected Trojan signal in the phased lightcurve of Kepler-25c. An Earth size Trojan (100ppm flux drop) is placed at L5 in the PDC flux data (detrended data with known systematics removed) and phased to show the host planetary transit and the Trojan at L5.The area around the L5 point is highlighted in the insert plot. The main figure shows the phased lightcurve with the injected Trojan. The shaded blue area represents the expected ±30° region where Trojans are expected, with the lowest gravitational potential point marked with dotted black lines.This data has been binned so that the planetary transit duration covers 3 bins, smoothing out short term variabilities in the data. The black horizontal line shows the mean of the data, and the red, green, and magenta show a 1,2, and 3σ deviation from the mean, respectively.

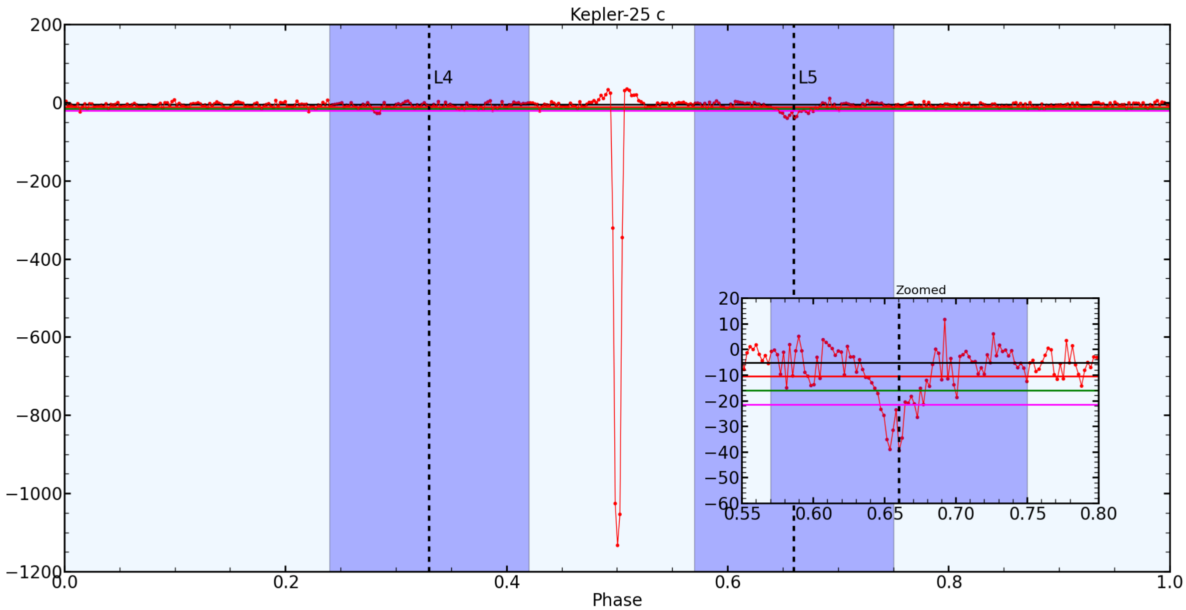

Figure 2.2.2: Injected Trojan signal with a libration amplitude of 0.04 (fraction of transit period) in the phased lightcurve of Kepler-25c. An Earth size Trojan (100ppm flux drop) is placed at L5 in the PDC flux dataset (detrended data with known systematics removed) and phased to show the host planetary transit and the Trojan at L5. The shaded blue area represents the ±30° region where Trojans are expected, with the lowest gravitational potential point marked with dotted black lines.This data has been binned so that the planetary transit duration covers 3 bins, smoothing out short term variabilities in the data. The area around the L5 point is highlighted in the insert plot. The black horizontal line shows the mean of the data, and the red, green, and magenta show a 1,2, and 3σ deviation from the mean, respectively

If exoplanetary science has taught us one thing, it is to expect the unexpected. It is entirely possible that a Trojan swarm may be much larger in number and collective mass than any swarm in our own Solar System. A Trojan swarm is typically not a homogeneous blob but has some density structure. Marzari et al. (2002) show the density structure of Jupiter's Trojans with inclinations <10°. This structure has been reproduced and added to the phased light curve of Kepler-25c in figure Figure 2.2.3

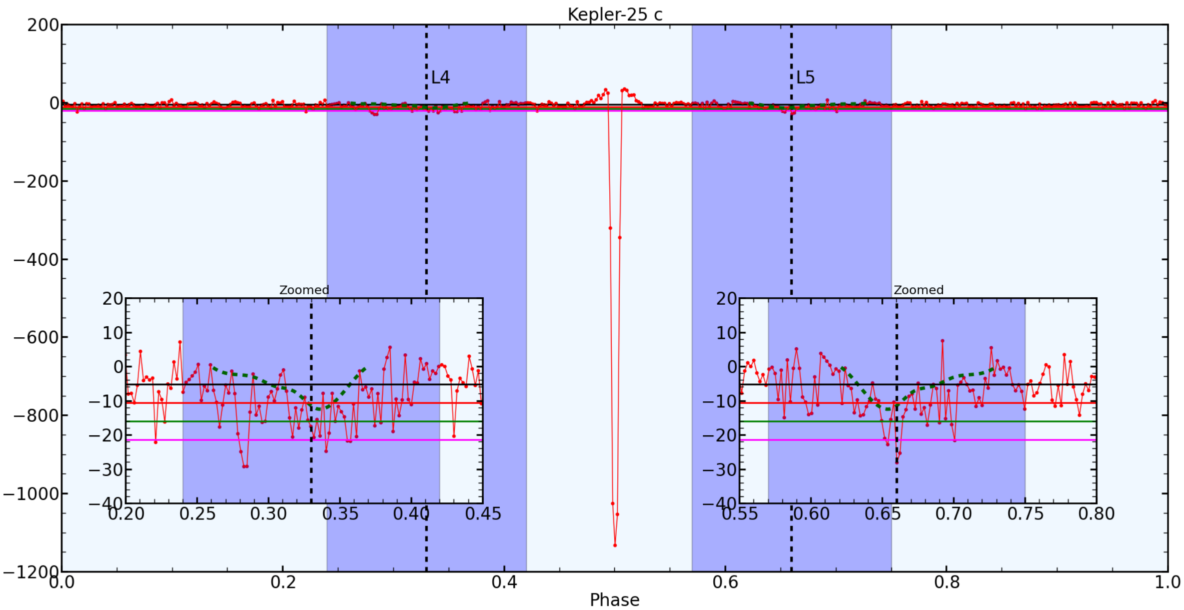

Figure 2.2.3: Injected Trojan swarm signal with a libration amplitude of 0.11 (fraction of transit period) in the phased lightcurve of Kepler-25c. An Trojan swarm is placed at L4 and L5 in the PDC flux data (detrended data with known systematics removed) and phased to show the host planetary transit and the Trojan swarms. Each transiting Trojan swarm has the collective radius of ~$1R_{\oplus}$. The Trojan swarms have a total angular spread of 0.11 (fraction of transit period) with the densest region located close to the respective L4 and L5 points. The Trojan cloud shape is based on Figure 3 in Marzari et al. (2002)'s paper (which describes the Jupiter trojan distribution) and are shown in dotted blue lines. The two insert figures highlight the Trojan clouds at L4 and L5. The shaded blue area represents the expected $\pm 30°$ region where Trojans are expected, with the lowest gravitational potential point marked with dotted black lines. This data has been binned so that the planetary transit duration covers 3 bins, smoothing out short term variabilities in the data.

The angular spread of Trojans swarms may also hinder their detection. A Trojan cloud size may be larger than the angular size of the star, meaning only a small fraction of the Trojan swarm may actually transit the star. Estimates from Moldovan et al. (2010) have shown that only a 5th of a swarm similar to Jupiter's Trojans would transit a star like HD209458. This does not reject the fact that exoplanetary Trojan swarms may be much larger in extent than those we see in our Solar system (see Figure 2.2.4).

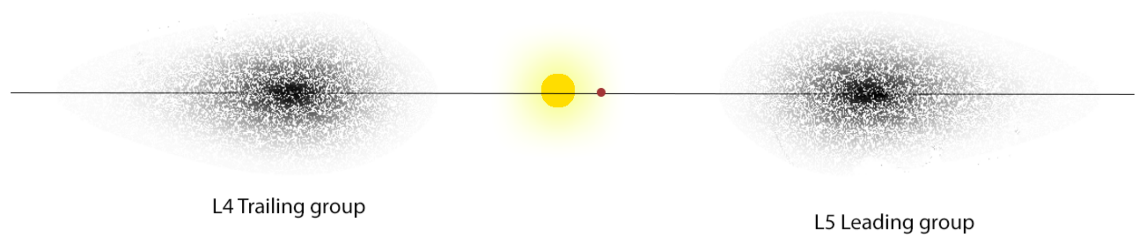

Figure 2.2.4: Schematic showing the angular extent of large Trojan swarm. Not to scale. Trojan swarm may appear out of transit with respect to the planet. This would produce only a fraction of the dimming expected if the entire swarm were transiting.

Chapter 3

Method

This section outlines the techniques and procedures used throughout this project.

3.1 Data Acquisition

To obtain the data, the *KPLR* python package was used. *KPLR* was created by Dan Foreman-Mackey and accesses the Mikulski Archive for Space Telescopes (*MAST*) data archive to download Kepler lightcurves. The PCD flux data was used in this project as the known systematic errors in the data are removed. Lightcurves of verified Kepler planets (Kepler objects - 2189 planets) and unconfirmed planets (KOI objects - 6637 planets) totalling 8826 planets, were downloaded with their corresponding fluxes, times and errors.

3.2 Removing other planets in multi-planetary transits

Before any analysis could be performed on the phased light curves of exoplanets to search for Trojans, it was essential to remove any other known transiting planetary bodies in the system. The *KPLR* package *star.kois* was used to identify any other known planets in the system. Knowing the planets T0 (time of first transit), period and duration, it was possible to find the transits in the lightcurve and remove those points in the lightcurve.

3.3 Phase folding and visual analysis

This analysis used the two complementary approaches of a visual inspection, and a systematic algorithmic search. Periodic signals can be folded according to their periods. This was done by taking the exoplanet's period, splitting the time series into chunks of that period, and folding the data onto itself. This can be seen in Figure 2.2.1 for example, with the planetary transit located at a phase of 0.5.

Before any detrending techniques were applied to the data (other than those already imparted to the PDC flux data), all 8826 planets' raw fluxes were visually inspected. To show the expected transiting regions of Trojans in phase space, shaded blue columns are introduced, representing the $\pm 30°$ potential regions of the Lagrange points. To test if a Trojan-like transit signal is statistically significant, lines of mean, 1σ, 2σ and 3σ were plotted, where 1σ represents 1 standard deviation in the out-of-planet and out-of-Trojan transit phases. Black vertically dashed lines are added to show the precise location of the lowest potential regions of L4 and L5 in the system (most likely places to find transiting Trojans). Once these guides were in place, each phased light curve was visually examined for transiting signals.

After the initial results were collected, a running median filter was applied to detrend the data in order to remove stellar variability (pulsating chromospheres, sunspots, flares, etc.). This detrending method takes 4 times the number of points taken for the transit to occur, i.e if the planet take 1.5 hours to transit, a running median of 6 hour bins was applied. This duration was taken to prevent the removal of the host planet transit itself or anything of a similar period. This is a powerful tool in detrending time series data. To test if this method actually improved the signal-to-noise of a Trojan transit, 3 types of Trojan signals were injected into the data, a single Trojan body of Earth Radius, a single Trojan of Earth radius librating about the L5 point and a Trojan swarm with the combined radius of a Earth size planet. Figure 3.3.1 shows the effectiveness of this detrending method. Transits that are undetectable in non-detrended data, become visually detectable after detrending. However, in the detrended data, we still see some dips that are equivalent in magnitude to the Trojan transit depth.

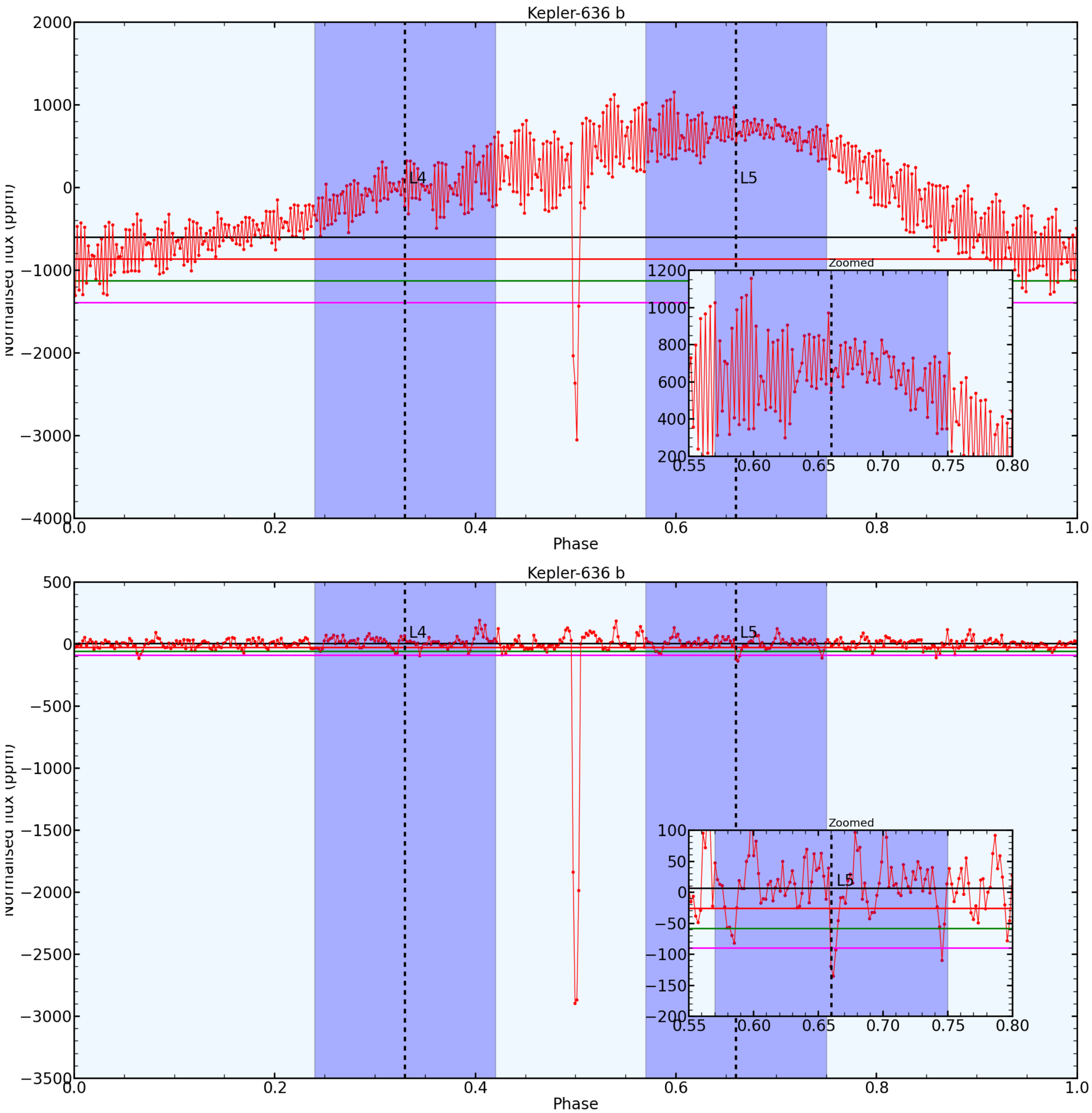

Figure 3.3.1: This figure shows the phased time series of Kepler-636b with an injected Trojan body at L5 with radius of 1 Earth.Top panel: Phased lightcurve of Kepler-636b unbinned with running median filter. Top panel insert: Trojan transit is clearly lost in the noise. Bottom panel: Phased lightcurve of Kepler-636b binned with a running median filter with 4 times the number of points in the transit duration. Bottom panel insert: Trojan transit is visible in the filtered data.

3.4 BLS analysis

The BLS (box-fitting least squares) periodogram analysis (Kovács et al., 2002) is an extremely useful and effective technique for detecting periodically transiting objects in a time series. This method looks for box-shaped dips in flux in photometric time series data. The box width can be adjusted to fit a given transit duration, while the period of the boxes can be also be made to fit the period of the transiting planet. This is commonly used to find transiting planets but may also be effective at detecting Trojan signals.

One problem with this method for detecting Trojan signals is that the Trojan (planet or swarm) and host planets' period will be very similar. This may wash out any Trojan signal and mask it as the host planet signal itself. However, since this method has proven to be extremely reliable at detecting planetary transits, it is wise to test this to detect Trojan transits.

It is assumed that the BLS technique will be more sensitive to large Trojan swarms rather than Trojan planets, because of the slight difference in period between large numbers of individual small Trojans, versus one signal large Trojan (ie. each individual trojan in a swarm will transit the host star at a different time than a single body. This frequency shift may favour detectability of a swarm over a single body using the BLS technique.). The change in period in Trojan swarms can be attributed to the libration amplitude, libration velocity and the eccentricity of the individual small Trojans. The variety in these parameters will have an effect on a transiting signal, distinguishing it from the host planet and may show up in the BLS test.

Before the BLS technique was used on the Kepler data to search for Trojans, a test was required to see if a Trojan signal could be detected and, if so, what would this detection look like in the periodogram. This test was done by injecting both a single Earth radius planet at the L5 position and a large Trojan swarm in the Kepler-636b lightcurve. The results of this test can be seen in Figure 3.4.1 and Figure 3.4.2 respectively.

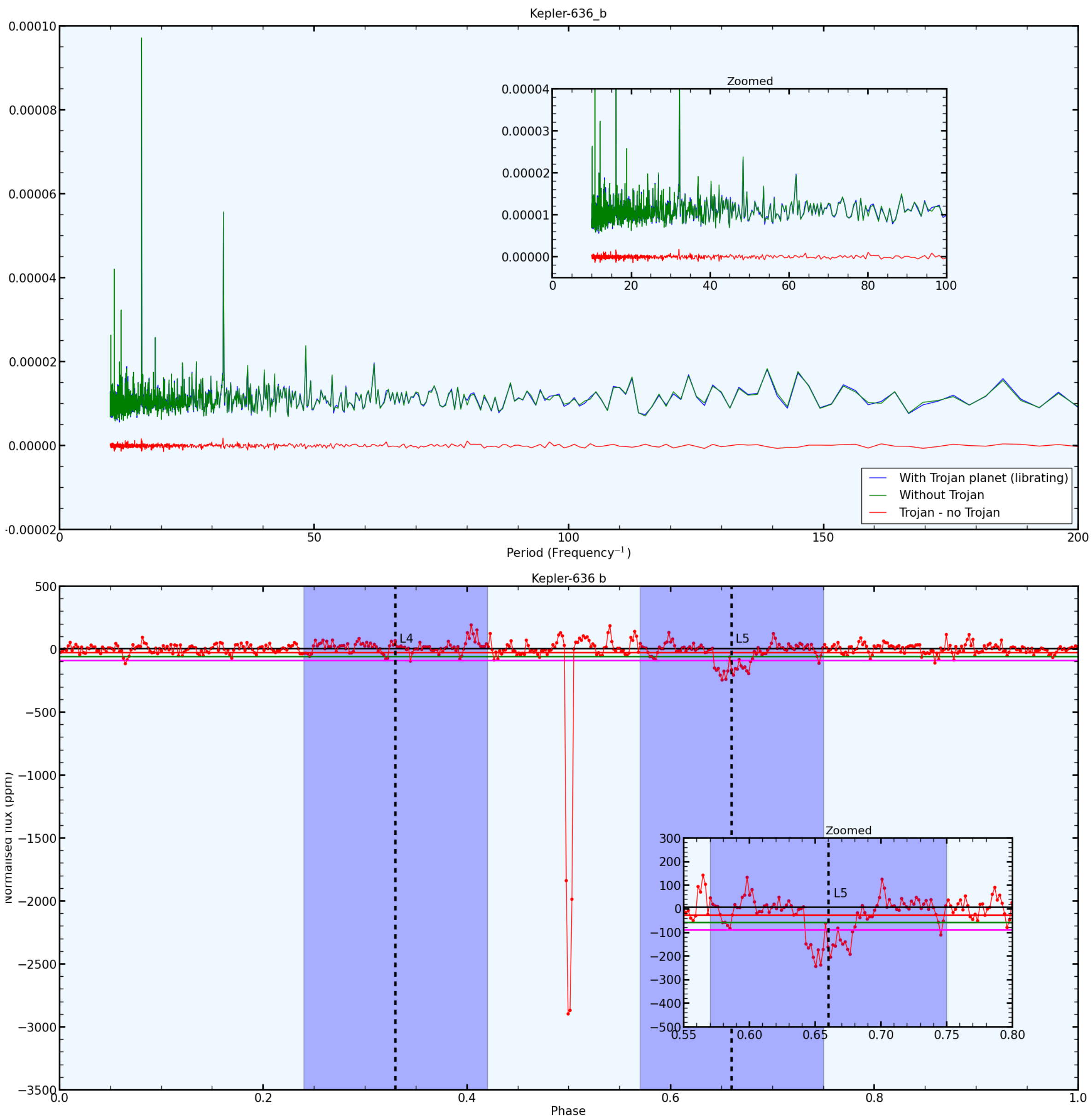

Figure 3.4.1: Top panel: BLS periodogram of Kepler-636b with no injected Trojan signal in green, a 1 Earth radius librating Trojan planet at L5 in blue and the Trojan signal alone in red. Bottom panel: Phase folded lightcurve of Kepler-636b with the same librating Trojan at L5.

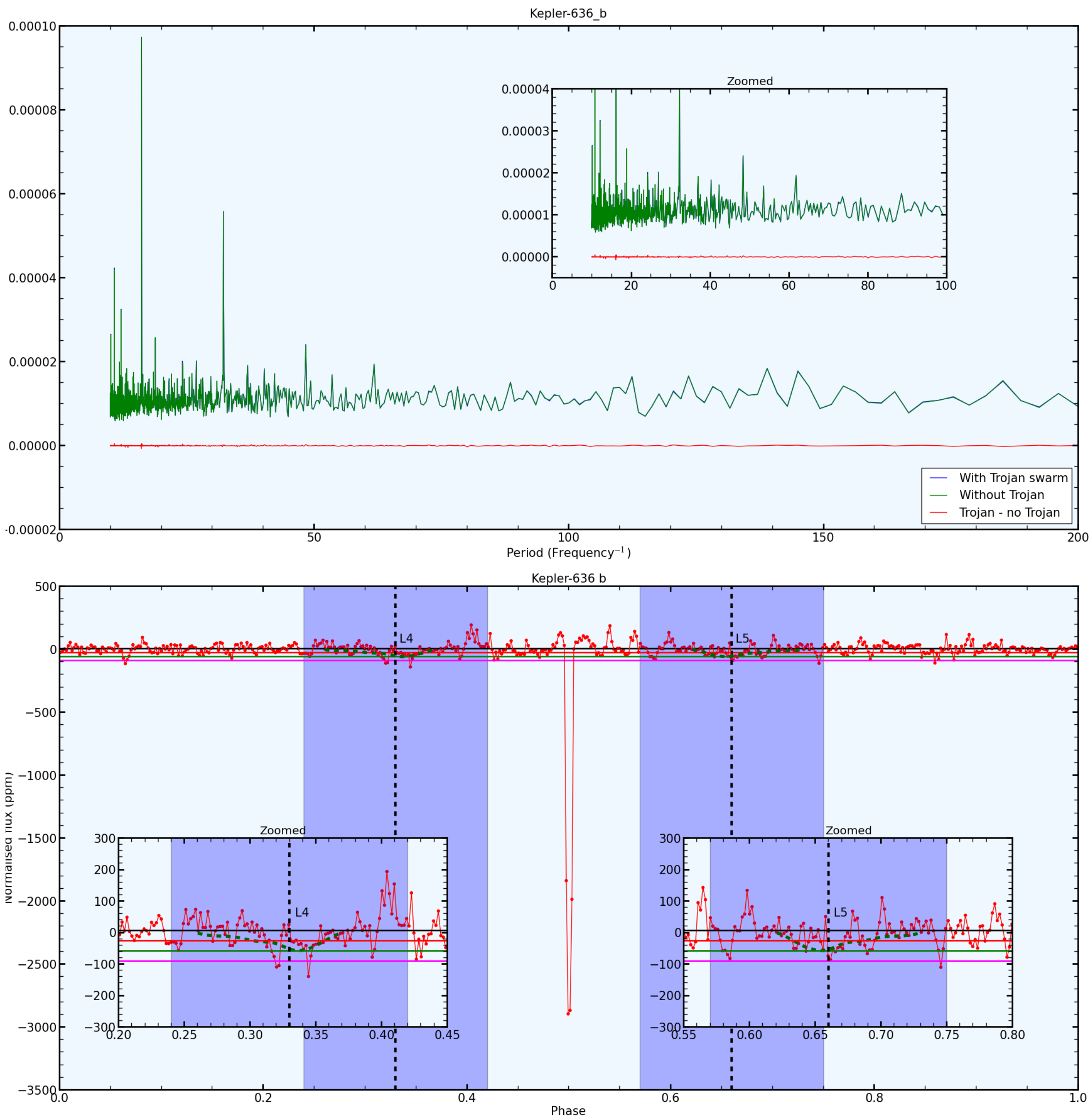

Figure 3.4.2: Top panel: BLS periodogram of Kepler-636b with no injected Trojan swarm signal in green, a Trojan swarm with the equivalent transiting area of a 1 Earth radius planet at L4 and L5 in blue and the Trojan swarm signal alone in red. Bottom panel: Phase folded lightcurve of Kepler-636b with the same Trojan swarm at L4 L5.

Figures 3.4.1 and 3.4.2 show how ineffective the BLS method is at detecting large librating Trojans or Trojan swarms. We see that the signal from the Trojan in blue, overlaps the signal without a Trojan. No features or peaks of the periodogram could reliably be attributed to a Trojan signal in several Kepler lightcurves with injected Trojan signals. It is for this reason the BLS technique was rejected as a suitable test to detect Trojans.

3.5 Fourier Analysis

This section describes a Fourier method used for detecting signals at specific frequencies in Fourier space in a non-uniform dataset.

Any time series data can be represented in Fourier space as a set of sines and cosines. This method can be very useful in determining the granulation process of a star, rotation periods of stars and detecting transiting exoplanets with a periodogram. Each frequency component can be disentangled into sines and cosines using the discrete Fourier transform (DFT), provided the time series is continuous and evenly sampled. This is not the case for Kepler data which, although evenly sampled, contains large gaps in time where the spacecraft required repositioning.

This was corrected by following a procedure outlined in Samsing (2015) which uses a Fourier least-squares matrix method to detect signals that are periodic and symmetric with respect to the planet transit, e.g. exoplanetary rings and Trojan swarms. This method has clear advantages over standard phase folding techniques as it can filter out all noise sources that are not periodic at (harmonics of) the orbital period including instrumental noise and stellar flux variations while also making it possible to resolve finer flux variations. Standard phase folding is only effective at reducing random noise.

This method is designed to find the best-fitting periodic model that is symmetric about the center of the transit, which is done by simultaneously fitting the sum of cosines that have periods that are integer fractions of the orbit. Separation of the noise and signal is possible because any signal associated with the transiting planet will be constrained to discrete and separate frequencies in the Fourier series, namely the cosine term. The cosine term is in phase with the transiting signal whereas the sine term will be out of phase with the transit but carries the information of the noise. It must be noted that this method is effective at detecting transit-symmetrical signals, this makes the method rather suited to Trojan swarms as they should show some symmetry with the host planet.

Step 1:
To effectively implement this method correctly, we must satisfy the condition that the signal be symmetric about the zero point (i.e. primary transit). This is done by cutting the data to a specific window which begins at the center of the first desired transit and ending at the center of the final desired transit.

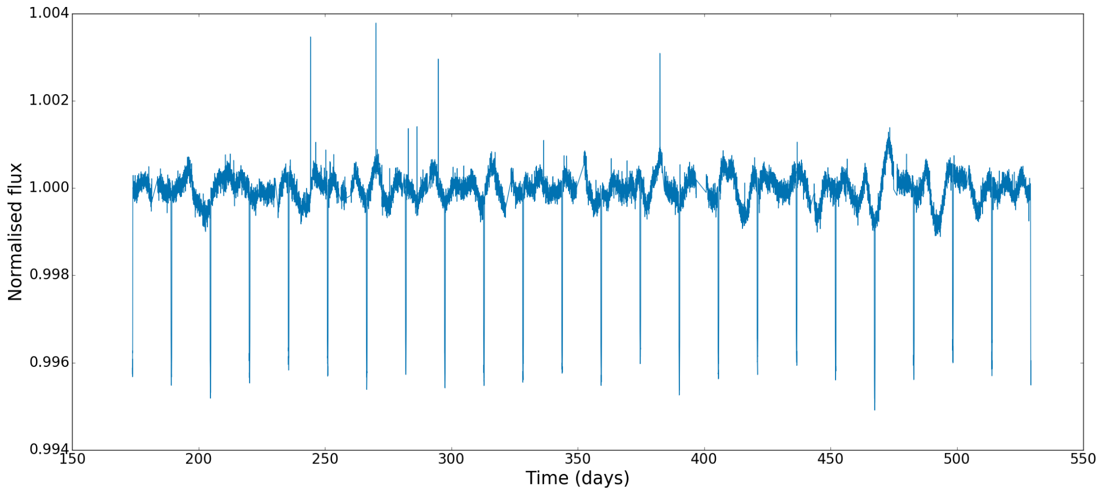

Figure 3.5.1: Data window of Kepler 628b starting from the first transit and ending at the 23rd transit. We see the effects of stellar variability causing variations in the data. We also see single bright points from day 240-400 possibly caused by cosmic rays hitting the sensor or stellar flares.

By cutting the data in this way, the cosine term fits the first and last transit, while also fitting everything at the same period as the planet. We can later extract the sine and cosine components of the Fourier series, where the transiting planet's signal and everything at that period is solely contained in the cosine component.

Step 2:
Next we must create a matrix array of phases (in radians) to fit the data. This ensures that we are indeed fitting periodic points in the data with the same period as the planet.

$$\phi = 2\pi\Big(\frac{ts - T_0}{T_w}\Big) \tag{3.5.1}$$

where ts is the time array, T_0 is the time of the first transit, at T_w is the length of the chosen window (in time). T_w should also be an integer number of planet periods, $T_w = N_0 P$, where N_0 is the number of transits and P is the planets period.

Step 3:
Once we have a matrix array of phases, we then create a new matrix by combining the cosine and sine components of the time array with the harmonics. This is done to create

a 2d column vector matrix of sines and cosines that we can use later to reconstruct the signal. This is the design matrix refereed to in Samsing (2015).

$$T_k = cos(\phi \cdot N) + sin(\phi \cdot N), \tag{3.5.2}$$

$$T_k = \underbrace{\begin{pmatrix} a_1, b_1 \\ a_2, b_2 \\ a_3, b_3 \\ a_4, b_4 \\ \ldots, \ldots \\ a_n, b_n \end{pmatrix}}_{\text{n=number of coefficients}} \tag{3.5.3}$$

where N is an integer array of harmonics from 1 to half the number of data points. T_k is equivalent to T_{ki} described in the appendix of Samsing (2015).

Step 4:
Next we need to calculate the a_n and b_n coefficients that match the data. These coefficients represent the amplitudes of the data at a given frequency in the fourier series.

$$R = \left({T_k}^T \cdot \ T_k\right)^{-1} \ {T_k}^T \cdot I \tag{3.5.4}$$

where the superscripted T here denotes the transpose and I is the intensity data. R is then an array of cosine and sine coefficients.

Step 5:
Separation of noise from signal can be done in this way because the window we chose minimises the overlap between signal and noise in Fourier Space. In this way, any information symmetric to the transit will be contained in a single frequency bin. We then remove the sine components as it only contains stellar noise (the cosine components contain information from the data at the frequency of the transiting planet, while the sine components contain all other frequency information, i.e. stellar noise). This is done by setting the second half of the R array to zero i.e. setting the b_n coefficients to zero. The first half of the array (the cosine component) contains all the information on the amplitude of the time series window at the frequency of the planet. The transiting signals occur at every N^{th} point in the cosine array where N is the number of transits observed in the windowed time series. This can be seen in Figure 3.5.2.

However, the inter-transit frequencies still contain some random stellar activity information, as this occurs on all frequencies. We can simply set the amplitude of these inter-transit frequencies to zero.

We also need to interpolate the time series in frequency space to normalise the cosine array. This is done by taking two points either side of the transit frequencies and subtracting the transit amplitude by the median of those two points.

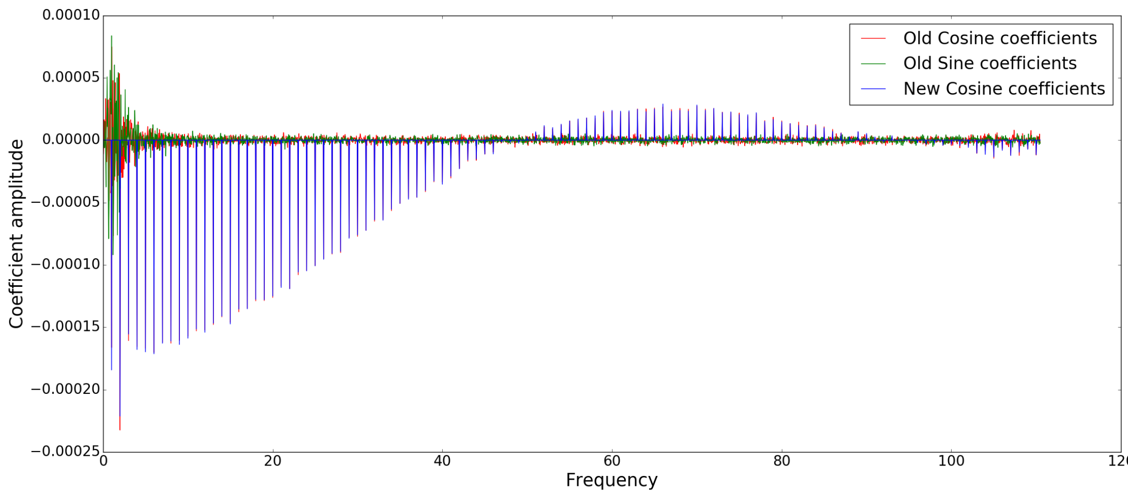

Figure 3.5.2: Fourier coefficient amplitude (R array) with the 'pre-cleaned' a_n coefficients in red, the b_n in green and the new, interpolated a_n coefficients in blue

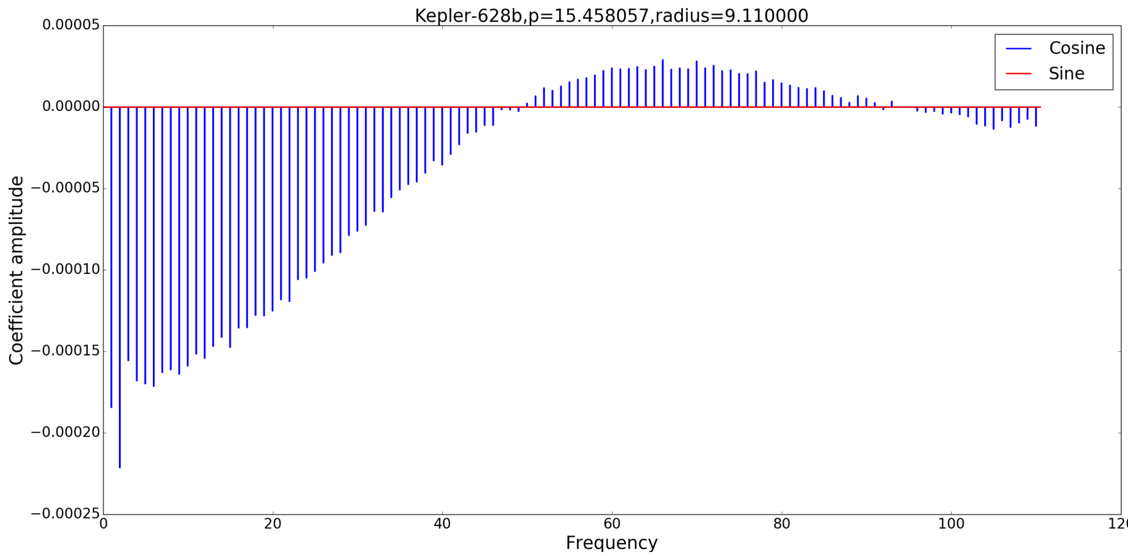

Figure 3.5.3: 'Cleaned' a_n cosine coefficients in blue and the sine coefficients (set to zero) in red

Step 6:

Once we have our 'cleaned' cosine and sine array (R), we can use the following equation to reconstruct the data with very little stellar contribution and only with frequencies of that of the planet's period:

$$I_{\text{new}} = T_k \cdot R \tag{3.5.5}$$

where I_{new} is the reconstructed data.

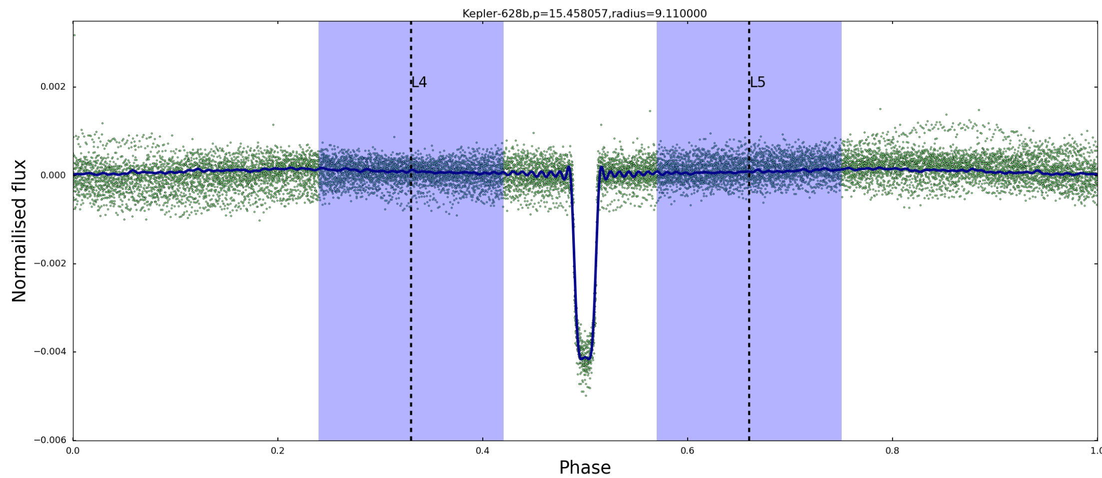

Figure 3.5.4: Reconstructed data from the cosine coefficients in blue (unbinned), with the original phased data in green dots (unbinned).

In Figure 3.5.4, we see the reconstructed data from the 'cleaned' Fourier cosine coefficients, which has a significantly lower noise component than the original data. Since the new data is not reconstructed with infinite Fourier coefficients, we see 'wiggles' due to the new signal reconstructed out of an incomplete set of frequencies. These are ringing artifacts that can be reduced to an arbitrarily small level by including an arbitrarily large number of terms. Due to time constraints, the number of coefficients was set to the number of points in the original windowed data.

The sine coefficients were also reconstructed in a separate test to ensure this method was performing the separation of stellar noise and transit signal successfully. This can be seen in Figure 3.5.5.

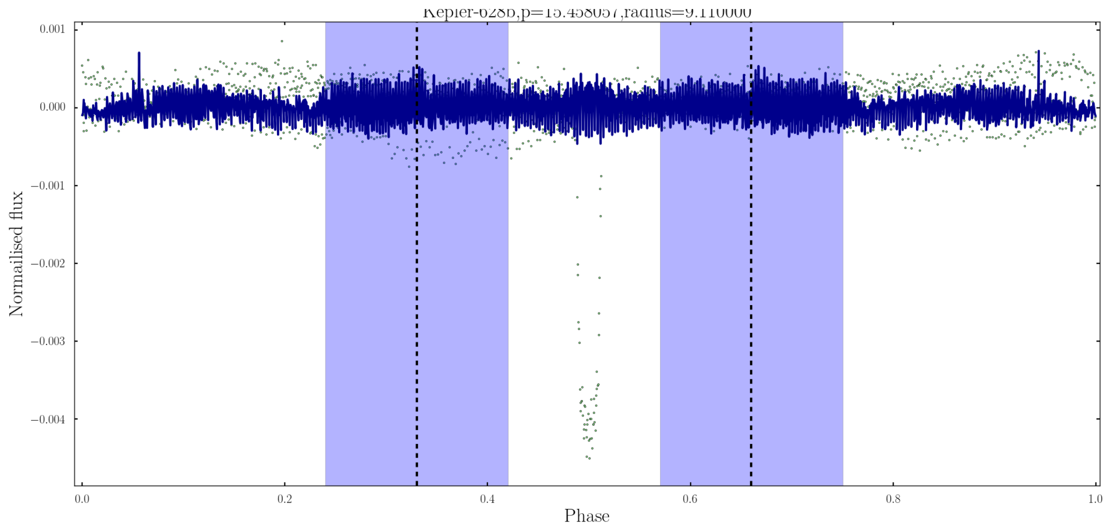

Figure 3.5.5: Reconstructed data from the sine coefficients in blue (unbinned), with the original phased data in green dots (unbinned).

We can see from Figure 3.5.5 and 3.5.4 that the separation of cosine and sine components was extremely successful.

Because this method can produce very large matrices (several million points in Step 4) it can be quite computationally time consuming. To rectify this issue, the time series data was binned to reduce the number of data points and only a selection of planets were chosen to perform this analysis. The planets selected are assumed to have favourable properties for Trojans to exist, with radii greater that $3R_{\oplus}$ (it is assumed that more massive planets will harbour larger Trojan swarms) and orbital periods greater than 100 days (under the assumption that larger orbital period planet have undergone less migration and thus, potentially less destructive to Trojan swarms than shorter period planets).

Another issue arose when performing the matrix multiplication in step 4, whereby the inverse matrix multiplication component contained zeros which creates degeneracies in the calculation. This was rectified by using the Python *numpy linalg* package *lstsq* which uses a Single Value Decomposition technique. This effectively ignores zeros and NANs in the matrix multiplication, breaking this degeneracy.

Once the data is reconstructed without correlated stellar activity contribution, we can run the previous algorithm (combined with visual inspection of the resulting reconstruction) to detect Trojan transits to a much higher precision.

Chapter 4

Results

In this section I will discuss the results I have obtained in this project, how effective the techniques were at detecting Trojan-like signals and where improvements can be made.

4.1 Phase folding and visual inspection results

Upon analysis of 8826 phased Kepler lightcurves (as described in section 2.1-2.3), some tentative Trojan candidates were detected. These candidates were compiled into a list for later inspection.

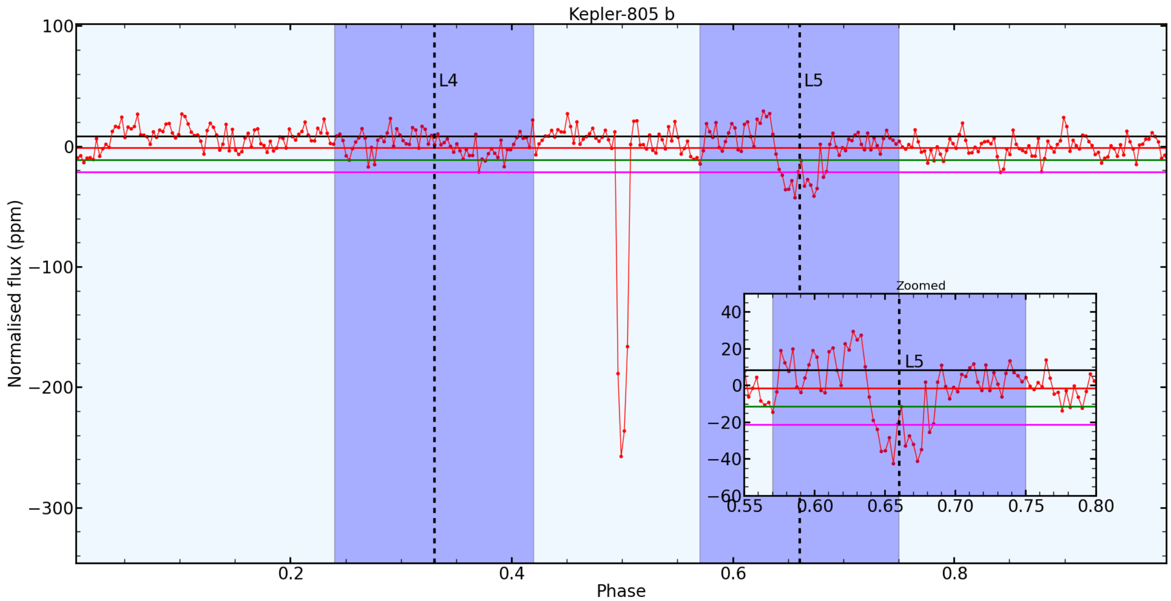

Figure 4.1.1: Example of a trojan candidate

In order to confirm these candidate Trojan transits were indeed transiting Trojan bodies, I first needed to rule out the possibility that these signals were caused by stellar noise, glitches in the data or effects introduced through the analysis process. Examining the un-phased lightcurves themselves proved extremely useful in identifying glitches in the Kepler data.

During its time in operation the Kepler spacecraft required repositioning, during which time no flux data was acquired. Often when the imaging system became operational again, a process known as charge trapping (where electrons can be trapped in the silicon lattice of the CCD) can form an artifact that can be seen in the data know as the “ramp effect”. This effect can be seen in Figure 4.1.2.

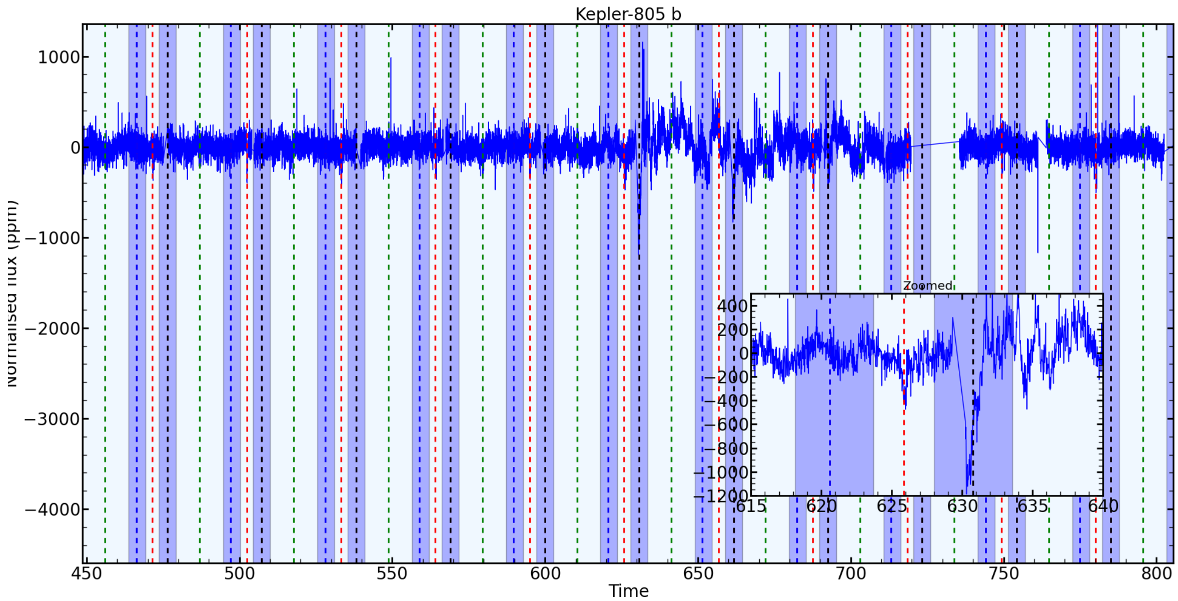

Figure 4.1.2: Example of the ramp effect seen in the Kepler 805b lightcurve. Planet transit marked in dashed red, L4 to the left, L5 to the right

When phasing up the flux data and binning it, this artifact can be confused with a transiting planet signal. This effect can sometimes be seen at exactly the L4 or L5 position, leading to a misidentification of a transiting Trojan. Once the Trojan candidate lightcurves were inspected, many of the candidates did indeed show this ramp effect as the cause for the misidentified transit (this was the case for Kepler-805b Figure 4.1.1).

Unfortunately, after extensive testing on all the confirmed Kepler objects and Kepler candidates, no significant evidence for Trojan planets or swarms were detected.

4.2 Fourier analysis results

To complete this analysis in a timely manner (given the large computing time of the large matrices involved), the process was optimised to search for Trojans in orbits greater than 100 days and planetary radii greater than 3 Earth radii. This selection contained 96 planets. An algorithm was set to search for three points below 3σ, where σ is defined as the standard deviation of the out-of-transit and out-of-Trojan transiting regions of the phased reconstructed data.

For planets with orbital periods greater than 100 days, there is a greater number of correlated frequency components (given a larger data window), which leads to the reconstruction of more noise than for reconstructed shorter period planet signals. This dampens the effectiveness of this method but still reduces a large number of correlated noise components in the dataset.

The selected 96 planets' Fourier reconstructed phased lightcurves showed no significant signs of any trojan swarms signal.

Placek et al. (2015) hinted at a potential trojan object around Kepler 91b. This was also tested with a Fourier least squares reconstruction. However, no statistically significant trojan signal was detected. The resulting reconstruction can be seen in Figure 4.2.1.

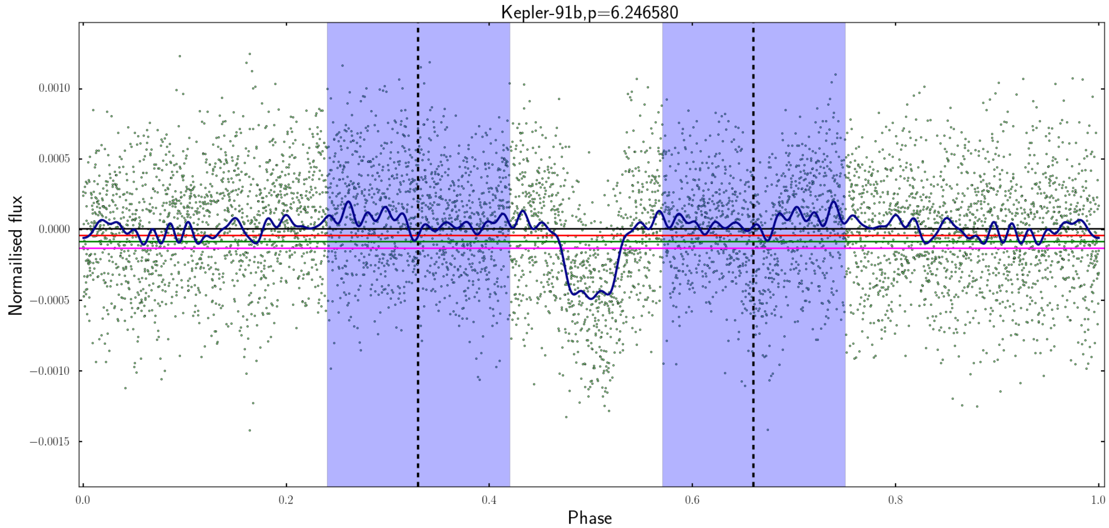

Figure 4.2.1: Reconstructed data from Kepler 91b cosine coefficients in blue (unbinned), with the original phased data in green dots (unbinned). The black horizontal line shows the mean of the reconstructed signal, and the red, green, and magenta show a 1,2, and 3σ deviation from the mean. No statitically significant trojan transit can be seen.

Chapter 5

Conclusion

The aim of this study was to detect individual large transiting Trojan bodies, be it a large Trojan planet or a large cluster of Trojan asteroids. While the phase folding and BLS analysis were both expected to be the most effect methods in detecting Trojan planets, it is evident from this research than no transiting Trojan planets are detectable in Kepler data. There are potentially many different explanations for this, but one interpretation of this result is that large Trojan planets are either extremely rare or smaller Trojan planets are more common but their librating motion makes them extremely difficult to detect.

The Fourier analysis test proved extremely effective for short period planets (approximately less than 30 days) but was slightly less effective for longer period planets due to the large size of the data window. It is unfortunate that this method is more sensitive to Trojan companions of shorter period planets as it is expected that large trojan swarms or planets are more likely to be stable at larger orbital distances from the host star (>0.5AU according to Cresswell and Nelson (2009)).

No significant individual trojan swarm were detected for the 96 planets with radii $>3R_\oplus$ and orbital periods >100 days in this analysis. I believe this is partly due to the large angular spread of Trojan swarms above and below the orbital plane (see Figure 2.2.4), where only part of the swarm transits the host star. One possibility is that the transiting swarms are not dense enough to produce a significant decrease in flux. This is expected as Jupiter's Trojan swarms would not be detectable in another solar system using Kepler data. Another potential reason is that the Yarkovsky effect is playing a role on the stability of trojan swarms, where radiation pressure may be pushing Trojans out of stable L4 and L5 points of planets with periods detectable in the Kepler dataset. This may suggest that no Trojans can exist within a certain distance from the host star, which may also effect the formation of Trojan planets. This mimics what we see in our Solar System. Mercury, Venus, Earth, and Mars have little to no Trojans, whereas Jupiter has ~6000 known Trojans. However, how stellar radiation effects the orbits of Trojan bodies has yet to be explored.

Perhaps this result points to a lack of large Asteroid or Kuiper belts in exoplanetary systems, which are thought to 'feed' the Jovian and Neptunian swarms.

Future missions like Plato will have a greater sensitivity than Kepler (27 ppm per hour (Rauer et al., 2014)) and survey even more stars for transiting planets, and potentially massive Trojan swarms or planets. The Fourier method described above may be instrumental in these future searches for Trojans or exoplanetary rings.

Bibliography

Pulliam C. Aguilar, D.A. At Least One in Six Stars Has an Earth-sized Planet. 2013.

T. Barclay, J. F. Rowe, J. J. Lissauer, D. Huber, F. Fressin, S. B. Howell, S. T. Bryson, W. J. Chaplin, J.-M. Désert, E. D. Lopez, G. W. Marcy, F. Mullally, D. Ragozzine, G. Torres, E. R. Adams, E. Agol, D. Barrado, S. Basu, T. R. Bedding, L. A. Buchhave, D. Charbonneau, J. L. Christiansen, J. Christensen-Dalsgaard, D. Ciardi, W. D. Cochran, A. K. Dupree, Y. Elsworth, M. Everett, D. A. Fischer, E. B. Ford, J. J. Fortney, J. C. Geary, M. R. Haas, R. Handberg, S. Hekker, C. E. Henze, E. Horch, A. W. Howard, R. C. Hunter, H. Isaacson, J. M. Jenkins, C. Karoff, S. D. Kawaler, H. Kjeldsen, T. C. Klaus, D. W. Latham, J. Li, J. Lillo-Box, M. N. Lund, M. Lundkvist, T. S. Metcalfe, A. Miglio, R. L. Morris, E. V. Quintana, D. Stello, J. C. Smith, M. Still, and S. E. Thompson. A sub-Mercury-sized exoplanet. *Nature*, 494:452–454, February 2013. doi: 10.1038/nature11914.

N. M. Batalha. Exploring exoplanet populations with NASA's Kepler Mission. *Proceedings of the National Academy of Science*, 111:12647–12654, September 2014. doi: 10.1073/pnas.1304196111.

A. Cassan, D. Kubas, J.-P. Beaulieu, M. Dominik, K. Horne, J. Greenhill, J. Wambsganss, J. Menzies, A. Williams, U. G. Jørgensen, A. Udalski, D. P. Bennett, M. D. Albrow, V. Batista, S. Brillant, J. A. R. Caldwell, A. Cole, C. Coutures, K. H. Cook, S. Dieters, D. Dominis Prester, J. Donatowicz, P. Fouqué, K. Hill, N. Kains, S. Kane, J.-B. Marquette, R. Martin, K. R. Pollard, K. C. Sahu, C. Vinter, D. Warren, B. Watson, M. Zub, T. Sumi, M. K. Szymański, M. Kubiak, R. Poleski, I. Soszynski, K. Ulaczyk, G. Pietrzyński, and Ł. Wyrzykowski. One or more bound planets per Milky Way star from microlensing observations. *Nature*, 481:167–169, January 2012. doi: 10.1038/nature10684.

D. Charbonneau, Z. K. Berta, J. Irwin, C. J. Burke, P. Nutzman, L. A. Buchhave, C. Lovis, X. Bonfils, D. W. Latham, S. Udry, R. A. Murray-Clay, M. J. Holman,

E. E. Falco, J. N. Winn, D. Queloz, F. Pepe, M. Mayor, X. Delfosse, and T. Forveille. A super-Earth transiting a nearby low-mass star. *Nature*, 462:891–894, December 2009. doi: 10.1038/nature08679.

M. Connors, P. Wiegert, and C. Veillet. Earth's Trojan asteroid. *Nature*, 475:481–483, July 2011. doi: 10.1038/nature10233.

P. Cresswell and R. P. Nelson. On the growth and stability of Trojan planets. *A&A*, 493:1141–1147, January 2009. doi: 10.1051/0004-6361:200810705.

A. Deprit and A. Deprit-Bartholome. Stability of the triangular Lagrangian points. *Aj*, 72:173, March 1967. doi: 10.1086/110213.

X. Dumusque, A. S. Bonomo, R. D. Haywood, L. Malavolta, D. Ségransan, L. A. Buchhave, A. Collier Cameron, D. W. Latham, E. Molinari, F. Pepe, S. Udry, D. Charbonneau, R. Cosentino, C. D. Dressing, P. Figueira, A. F. M. Fiorenzano, S. Gettel, A. Harutyunyan, K. Horne, M. Lopez-Morales, C. Lovis, M. Mayor, G. Micela, F. Motalebi, V. Nascimbeni, D. F. Phillips, G. Piotto, D. Pollacco, D. Queloz, K. Rice, D. Sasselov, A. Sozzetti, A. Szentgyorgyi, and C. Watson. The Kepler-10 Planetary System Revisited by HARPS-N: A Hot Rocky World and a Solid Neptune-Mass Planet. *ApJ*, 789:154, July 2014. doi: 10.1088/0004-637X/789/2/154.

R. Dvorak, E. Pilat-Lohinger, R. Schwarz, and F. Freistetter. Extrasolar Trojan planets close to habitable zones. *A&A*, 426:L37–L40, November 2004. doi: 10.1051/0004-6361:200400075.

exoplanetarchive. 1 exoplanetarchive.ipac.caltech.edu @MISC. URL `exoplanetarchive.ipac.caltech.edu`. Accessed: 2017-08-28.

Y. R. Fernández, S. S. Sheppard, and D. C. Jewitt. The Albedo Distribution of Jovian Trojan Asteroids. *Aj*, 126:1563–1574, September 2003. doi: 10.1086/377015.

E.B. Ford. Architectures of Planetary Systems and Implications for their Formation. *PNAS*, 111:1261612621, April 2014. doi: 10.1073/pnas.1304219111.

M. Fridlund, E. Gaidos, O. Barragán, C. M. Persson, D. Gandolfi, J. Cabrera, T. Hirano, M. Kuzuhara, S. Csizmadia, G. Nowak, M. Endl, S. Grziwa, J. Korth, J. Pfaff, B. Bitsch, A. Johansen, A. J. Mustill, M. B. Davies, H. J. Deeg, E. Palle, W. D. Cochran, P. Eigmüller, A. Erikson, E. Guenther, A. P. Hatzes, A. Kiilerich, T. Kudo, P. MacQueen, N. Narita, D. Nespral, M. Pätzold, J. Prieto-Arranz, H. Rauer, and V. Van Eylen. K2-111 b - a short period super-Earth transiting a metal poor, evolved old star. *A&A*, 604:A16, July 2017. doi: 10.1051/0004-6361/201730822.

B. Scott. Gaudi, K. Stassun, and K. Collins. A giant planet undergoing extreme-ultraviolet irradiation by its hot massive-star host. *Nature*, 2017. doi: 10.1038/nature22392.

M. Gillon, D. R. Anderson, A. Collier-Cameron, L. Delrez, C. Hellier, E. Jehin, M. Lendl, P. F. L. Maxted, F. Pepe, D. Pollacco, D. Queloz, D. Ségransan, A. M. S. Smith, B. Smalley, J. Southworth, A. H. M. J. Triaud, S. Udry, V. Van Grootel, and R. G. West. WASP-103 b: a new planet at the edge of tidal disruption. *A&A*, 562: L3, February 2014. doi: 10.1051/0004-6361/201323014.

C. Hellier, D. R. Anderson, A. C. Cameron, L. Delrez, M. Gillon, E. Jehin, M. Lendl, P. F. L. Maxted, F. Pepe, D. Pollacco, D. Queloz, D. Ségransan, B. Smalley, A. M. S. Smith, J. Southworth, A. H. M. J. Triaud, S. Udry, and R. G. West. Transiting hot Jupiters from WASP-South, Euler and TRAPPIST: WASP-95b to WASP-101b. *MNRAS*, 440:1982–1992, May 2014. doi: 10.1093/mnras/stu410.

M. Hippke and D. Angerhausen. A Statistical Search for a Population of Exo-Trojans in the Kepler Data Set. *ApJ*, 811:1, September 2015. doi: 10.1088/0004-637X/811/1/1.

M. Janson. A Systematic Search for Trojan Planets in the Kepler Data. *ApJ*, 774:156, September 2013. doi: 10.1088/0004-637X/774/2/156.

D. C. Jewitt, C. A. Trujillo, and J. X. Luu. Population and Size Distribution of Small Jovian Trojan Asteroids. *Aj*, 120:1140–1147, August 2000. doi: 10.1086/301453.

D. M. Kipping, D. Nesvorný, L. A. Buchhave, J. Hartman, G. Á. Bakos, and A. R. Schmitt. The Hunt for Exomoons with Kepler (HEK). IV. A Search for Moons around Eight M Dwarfs. *ApJ*, 784:28, March 2014. doi: 10.1088/0004-637X/784/1/28.

D. G. Koch, W. J. Borucki, G. Basri, N. M. Batalha, T. M. Brown, D. Caldwell, J. Christensen-Dalsgaard, W. D. Cochran, E. DeVore, E. W. Dunham, T. N. Gautier, III, J. C. Geary, R. L. Gilliland, A. Gould, J. Jenkins, Y. Kondo, D. W. Latham, J. J. Lissauer, G. Marcy, D. Monet, D. Sasselov, A. Boss, D. Brownlee, J. Caldwell, A. K. Dupree, S. B. Howell, H. Kjeldsen, S. Meibom, D. Morrison, T. Owen, H. Reitsema, J. Tarter, S. T. Bryson, J. L. Dotson, P. Gazis, M. R. Haas, J. Kolodziejczak, J. F. Rowe, J. E. Van Cleve, C. Allen, H. Chandrasekaran, B. D. Clarke, J. Li, E. V. Quintana, P. Tenenbaum, J. D. Twicken, and H. Wu. Kepler Mission Design, Realized Photometric Performance, and Early Science. *ApJ*, 713:L79-L86, April 2010. doi: 10.1088/2041-8205/713/2/L79.

G. Kovács, S. Zucker, and T. Mazeh. A box-fitting algorithm in the search for periodic transits. *A&A*, 391:369–377, August 2002. doi: 10.1051/0004-6361:20020802.

L. Kreidberg, J. L. Bean, J.-M. Désert, B. Benneke, D. Deming, K. B. Stevenson, S. Seager, Z. Berta-Thompson, A. Seifahrt, and D. Homeier. Clouds in the atmosphere of the super-Earth exoplanet GJ1214b. *Nature*, 505:69–72, January 2014. doi: 10.1038/nature12888.

G. Laughlin and J. E. Chambers. Extrasolar Trojans: The Viability and Detectability of Planets in the 1:1 Resonance. *Aj*, 124:592–600, July 2002. doi: 10.1086/341173.

J. J. Lissauer, D. Ragozzine, D. C. Fabrycky, J. H. Steffen, E. B. Ford, J. M. Jenkins, A. Shporer, M. J. Holman, J. F. Rowe, E. V. Quintana, N. M. Batalha, W. J. Borucki, S. T. Bryson, D. A. Caldwell, J. A. Carter, D. Ciardi, E. W. Dunham, J. J. Fortney, T. N. Gautier, III, S. B. Howell, D. G. Koch, D. W. Latham, G. W. Marcy, R. C. Morehead, and D. Sasselov. Architecture and Dynamics of Kepler's Candidate Multiple Transiting Planet Systems. *ApJs*, 197:8, November 2011. doi: 10.1088/0067-0049/197/1/8.

P. S. Lykawka and J. Horner. The capture of Trojan asteroids by the giant planets during planetary migration. *MNRAS*, 405:1375–1383, June 2010. doi: 10.1111/j.1365-2966.2010.16538.x.

W. Lyra, A. Johansen, H. Klahr, and N. Piskunov. Standing on the shoulders of giants. Trojan Earths and vortex trapping in low mass self-gravitating protoplanetary disks of gas and solids. *A&A*, 493:1125–1139, January 2009. doi: 10.1051/0004-6361:200810797.

L. MacLachlan. The Trials of Giordano Bruno: Links and Bibliography. URL `http://www.famous-trials.com/bruno/264-bibliography`.

F. Marzari, H. Scholl, C. Murray, and C. Lagerkvist. *Origin and Evolution of Trojan Asteroids*, pages 725–738. March 2002.

F. S. Masset and J. C. B. Papaloizou. Runaway Migration and the Formation of Hot Jupiters. *ApJ*, 588:494–508, May 2003. doi: 10.1086/373892.

M. Mayor and D. Queloz. A Jupiter-mass companion to a solar-type star. 378:355–359, November 1995. doi: 10.1038/378355a0.

R. Moldovan, J.M. Matthews, B. Gladman, W.F. Bottke, and D. Vokrouhlick. Searching for Trojan Asteroids in the HD 209458 System: Space-based MOST Photometry and Dynamical Modeling. *ApJ*, 716:315–323, June 2010. doi: 10.1088/0004-637X/716/1/315.

Levison H. F. Tsiganis K Gomes R Morbidelli, A. Chaotic capture of Jupiter's Trojan asteroids in the early Solar System. *Nature*, 435:462–465, May 2005. doi: doi:10.1038/nature03540.

M. Nagasawa, S. Ida, and T. Bessho. Formation of Hot Planets by a Combination of Planet Scattering, Tidal Circularization, and the Kozai Mechanism. *ApJ*, 678: 498-508, May 2008. doi: 10.1086/529369.

URL `"www.nasa.gov/mission`$_{p}ages/kepler/spacecraft/index.html". \ Accessed \ : 2018-07-01.$

B. Placek, K. H. Knuth, D. Angerhausen, and J. M. Jenkins. Characterization of Kepler-91b and the Investigation of a Potential Trojan Companion Using EXONEST. *ApJ*, 814:147, December 2015. doi: 10.1088/0004-637X/814/2/147.

H. Rauer, C. Catala, C. Aerts, T. Appourchaux, W. Benz, A. Brandeker, J. Christensen-Dalsgaard, M. Deleuil, L. Gizon, M.-J. Goupil, M. Güdel, E. Janot-Pacheco, M. Mas-Hesse, I. Pagano, G. Piotto, D. Pollacco, Ċ. Santos, A. Smith, J.-C. Suárez, R. Szabó, S. Udry, V. Adibekyan, Y. Alibert, J.-M. Almenara, P. Amaro-Seoane, M. A.-v. Eiff, M. Asplund, E. Antonello, S. Barnes, F. Baudin, K. Belkacem, M. Bergemann, G. Bihain, A. C. Birch, X. Bonfils, I. Boisse, A. S. Bonomo, F. Borsa, I. M. Brandão, E. Brocato, S. Brun, M. Burleigh, R. Burston, J. Cabrera, S. Cassisi, W. Chaplin, S. Charpinet, C. Chiappini, R. P. Church, S. Csizmadia, M. Cunha, M. Damasso, M. B. Davies, H. J. Deeg, R. F. Díaz, S. Dreizler, C. Dreyer, P. Eggenberger, D. Ehrenreich, P. Eigmüller, A. Erikson, R. Farmer, S. Feltzing, F. de Oliveira Fialho, P. Figueira, T. Forveille, M. Fridlund, R. A. García, P. Giommi, G. Giuffrida, M. Godolt, J. Gomes da Silva, T. Granzer, J. L. Grenfell, A. Grotsch-Noels, E. Günther, C. A. Haswell, A. P. Hatzes, G. Hébrard, S. Hekker, R. Helled, K. Heng, J. M. Jenkins, A. Johansen, M. L. Khodachenko, K. G. Kislyakova, W. Kley, U. Kolb, N. Krivova, F. Kupka, H. Lammer, A. F. Lanza, Y. Lebreton, D. Magrin, P. Marcos-Arenal, P. M. Marrese, J. P. Marques, J. Martins, S. Mathis, S. Mathur, S. Messina, A. Miglio, J. Montalban, M. Montalto, M. J. P. F. G. Monteiro, H. Moradi, E. Moravveji, C. Mordasini, T. Morel, A. Mortier, V. Nascimbeni, R. P. Nelson, M. B. Nielsen, L. Noack, A. J. Norton, A. Ofir, M. Oshagh, R.-M. Ouazzani, P. Pápics, V. C. Parro, P. Petit, B. Plez, E. Poretti, A. Quirrenbach, R. Ragazzoni, G. Raimondo, M. Rainer, D. R. Reese, R. Redmer, S. Reffert, B. Rojas-Ayala, I. W. Roxburgh, S. Salmon, A. Santerne, J. Schneider, J. Schou, S. Schuh, H. Schunker, A. Silva-Valio, R. Silvotti, I. Skillen, I. Snellen, F. Sohl, S. G. Sousa, A. Sozzetti, D. Stello, K. G. Strassmeier, M. Švanda, G. M. Szabó, A. Tkachenko, D. Valencia, V. Van Grootel, S. D. Vauclair, P. Ventura, F. W. Wagner, N. A. Walton, J. Weingrill, S. C. Werner, P. J. Wheatley, and K. Zwintz. The PLATO 2.0 mission. *Experimental Astronomy*, 38:249–330, November 2014. doi: 10.1007/s10686-014-9383-4.

J. Samsing. Extracting Periodic Transit Signals from Noisy Light Curves using Fourier Series. *ApJ*, 807:65, July 2015. doi: 10.1088/0004-637X/807/1/65.

R. Schwarz and R. Dvorak. Trojan capture by terrestrial planets. *Celestial Mechanics and Dynamical Astronomy*, 113:23–34, May 2012. doi: 10.1007/s10569-012-9404-4.

S. Sheppard and C. Trujillo. Detection of a Trailing (L5) Neptune Trojan. *Science Express*, 2010.

A. Vidal-Madjar, A. Lecavelier des Etangs, J.-M. Désert, G. E. Ballester, R. Ferlet, G. Hébrard, and M. Mayor. An extended upper atmosphere around the extrasolar planet HD209458b. *Nature*, 422:143–146, March 2003. doi: 10.1038/nature01448.

F. Yoshida and T. Nakamura. Size Distribution of Faint Jovian L4 Trojan Asteroids. *Aj*, 130:2900–2911, December 2005. doi: 10.1086/497571.